CHAPTER 6

Synthesis, application and optimization studies of polyaniline/activated carbon/copper ferrite based composite material

6.1 Introduction

In the previous chapter (chapter 5), it was observed that the ternary composite PANI/AC/CoF demonstrated better electrochemical behavior as compared to pristine PAN and binary composite materials PANI/AC and PANI/CoF. The ternary composite PANI/AC/CoF was further optimized in terms of the weight ratio of the constituent components for the best specific capacitance. The current chapter also comprises two parts. In part, I, another novel low-cost composite material containing polyaniline-activated carbon-copper ferrite (PANI/AC/CuF) has been prepared for use in supercapacitor electrode applications. Also, a comparison of the electrochemical performances of pristine polyaniline (PANI), binary polyaniline-activated carbon (PANI/AC), and binary polyaniline- copper ferrite (PANI/CuF) has been discussed in contrast to the ternary composite material. For the synthesis of PANI, 9.40 g of aniline monomer along with 28.5 g of ammonium persulfate and 8.61 g of p-toluene sulfonic acid was taken. For the preparation of binary and ternary composite materials, 2.30 g of activated carbon and 2.3 g of copper ferrite was used so that the corresponding weight ratio in the composite materials is 4:1 (PANI: AC), 4:1 (PANI/CuF) and 4:1:1 (PANI/AC/CuF), respectively.

In part II, the optimization studies of the ternary composite material have been discussed in order to determine the best composition towards the best electrochemical properties.

Part I: Electrochemical performance of pristine PANI, binary PANI/AC, binary PANI/CuF, and ternary composite PANI/AC/CuF.

6.2 Result and discussion

6.2.1 X-ray diffraction

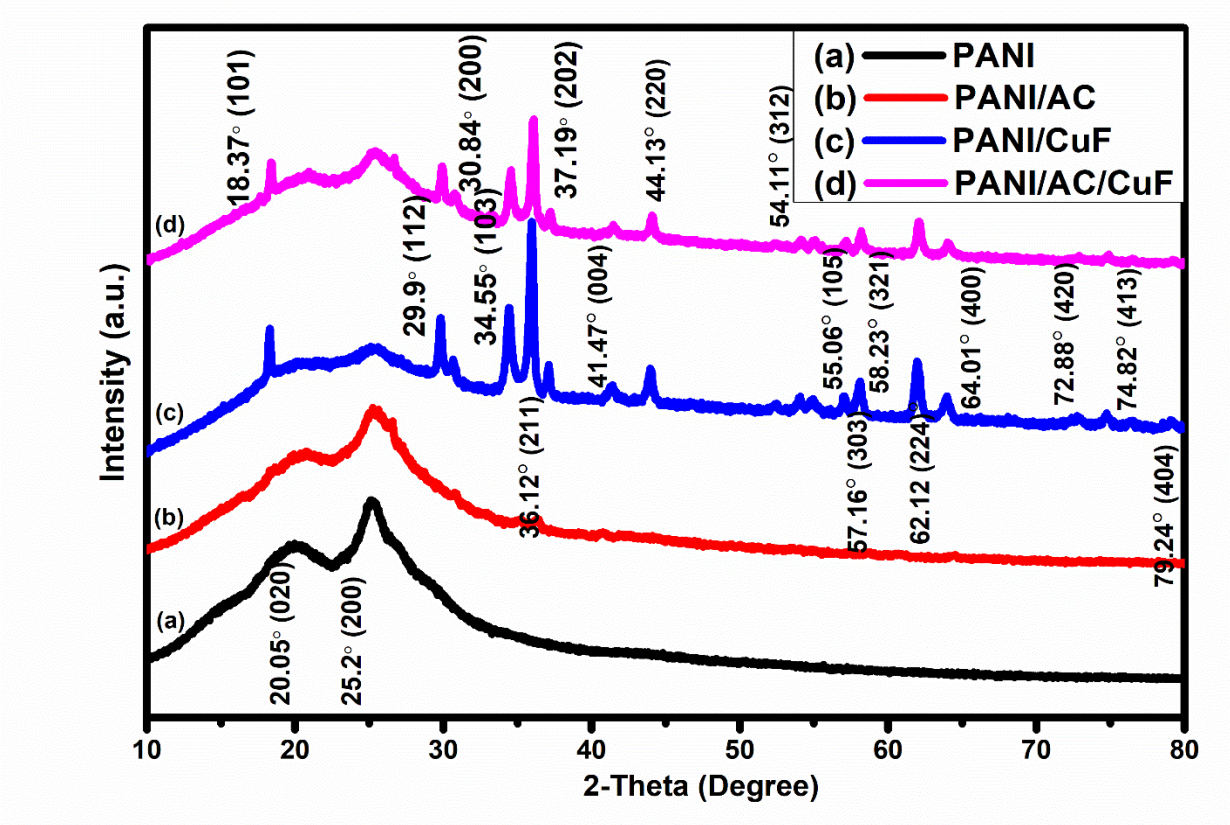

Fig 6.1: XRD patterns of pristine PANI, binary PANI/AC, binary PANI/CuF, and ternary PANI/AC/CuF

The XRD spectra were employed to confirm the successful synthesis of the synthesized materials. Figure 6.1 manifests the XRD patterns of pristine polyaniline (PANI), binary polyaniline-activated carbon (PANI/AC), binary polyaniline-copper ferrite (PANI/CuF), and ternary polyaniline-activated carbon-copper ferrite (PANI/AC/CuF). The synthesis of PANI was confirmed by humps at 20.05° (020) and 25.2° (200) [248]. The characteristic diffraction peak of AC (Fig. A1 (A) in appendix) may have merged to form a single peak at 25.2° in the case of binary PANI/AC. The diffraction present at 18.28° (101), 29.85° (112), 30.79° (200), 34.55 (103), 36.1° (211), 37.2° (202), 41.34 (004), 44.00° (220), 54.02 (312), 54.95° (105), 57.06 (303), 58.15° (321), 62.06° (224), 64.02° (400), 72.94° (420), 74.88° (413) and 79.1 (404) indicate a successful synthesis of copper ferrite particles (JCPDS 34-0425) (Fig. A1 (D) in appendix). A crystalline size of 33.8 nm was obtained as calculated with the help of Bragg's

formula (eq. 3.5). The peaks present at 18.37° (101), 29.9° (112), 30.84° (200), 34.55° (103), 36.12° (211), 37.19° (202), 41.47° (004), 44.13° (220), 54.11° (312), 55.06° (105), 57.16° (303), 58.23° (321), 62.12° (224), 64.01° (400), 72.88° (420), 74.82° (413) and 79.24° (404) confirmed the presence of CuF particles in PANI to form PANI/CuF. Further, all the expected spikes of PANI, PANI/AC, and PANI/CuF could be observed in the ternary composite PANI/AC/CuF with little shifting to mark its successful synthesis. Similar XRD patterns were also observed in the case of previously prepared ternary composites PANI/AC/CuCo and PANI/AC/CoF.

6.2.2 FTIR

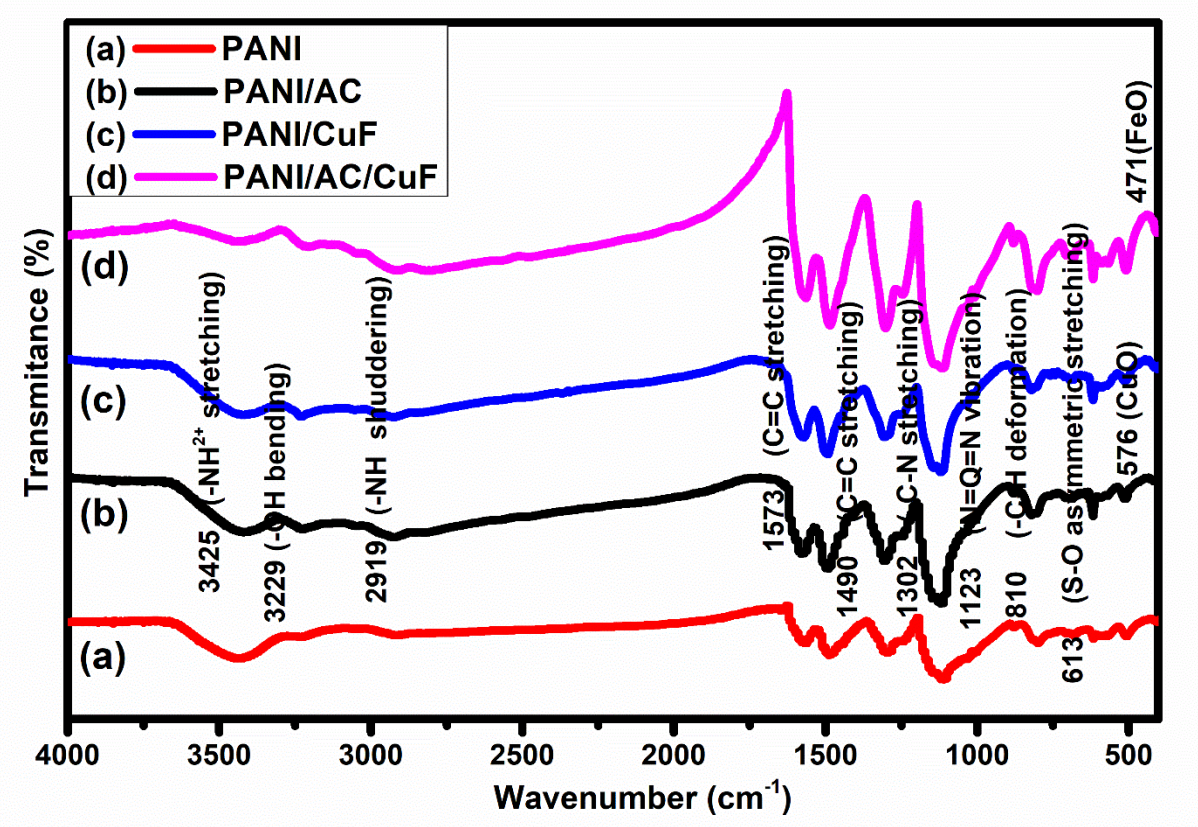

Fig 6.2: FTIR spectra of pristine PANI, binary PANI/AC, binary PANI/CuF, and ternary PANI/AC/CuF

The FTIR spectra for the prepared samples were recorded and have been presented in figure 6.2. For PANI, the band at 3425 cm^{-1} was associated with $-NH^{2+,}$ and -OH bending was indicated by the band at 3229 cm^{-1} [228,229]. The band at 2919 cm^{-1} was present due to -NH vibrations [228]. The impressions at 1573 cm^{-1} was attributed to quinoid rings and that at 1490 cm^{-1} to benzoid ring C=C vibrational stretching. The presence of PANI in benzoid form is in higher amounts due to the presence of its more intense absorption band, especially in the case of ternary composite material. The C-N vibrations were indicated at 1302 cm^{-1} due to the presence of protonated PANI. The p-substituted group with N=Q=N stretching vibrations in the case of PANI was present at 1123 cm^{-1}. This strong characteristic band is considered to behave as 'electron-like band' and is a measure of delocalization of electrons, and therefore indicates the conductivity of PANI. The band at 810 cm^{-1} was attributed to -CH deformation indicating the presence of PTSA in PANI [231]. The characteristic band of AC at 1070 cm^{-1} is responsible for π-π* interactions between AC particles and aniline monomer, and therefore the incorporation of PANI with AC improves the stability, functionality, and conductivity of its composite materials. The $-SO_3$ asymmetric vibration of PANI was marked by the peak at 613 cm^{-1}. In the case of binary PANI/CuF, bands at 576 and 471 cm^{-1} indicated the presence of Cu-O and Fe-O. All the expected bands in the ternary composite PANI/AC/CuF could be distinguished with little shifting. Further, Similar FTIR patterns were also observed in the case of previously prepared ternary composites PANI/AC/CuCo and PANI/AC/CoF.

6.2.3 Morphological analysis

The FESEM images for pristine PANI, binary PANI/AC, binary PANI/CuF, and ternary PANI/AC/CuF have been presented in figure 6.3. PANI manifests mostly rod-like structures, which are interconnected. In the case of binary PANI/AC, these rod-like structures are visible, but there is unevenness due to the presence of AC. In the case of binary PANI/CuF, some agglomeration could be observed due to the conversion of the micelle-like PTSA-aniline

complex into nanorods. In the case of ternary PANI/AC/CuF ternary composite, compact and rod-like clusters are mostly present due to activated carbon and copper ferrite particles with little agglomeration. Similar, rod-like structures with some agglomeration was also observed in the previously prepared ternary composite materials PANI/AC/CuCo and PANI/AC/CoF. FESEM micrographs of AC and CuF have been presented in fig. A3 (appendix).

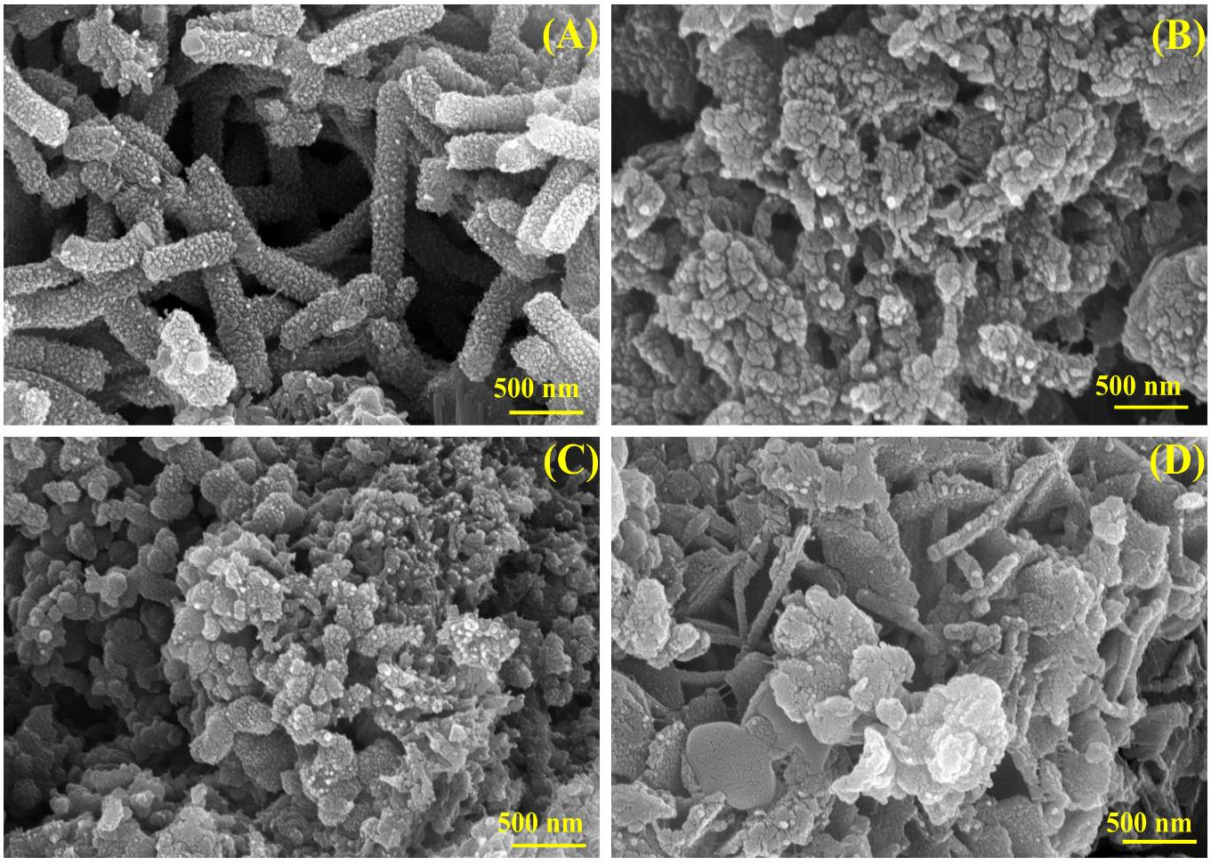

Fig 6.3: FESEM micrographs of (A) PANI, (B) PANI/AC, (C) PANI/CuF, and (D) PANI/AC/CuF

6.2.4 EDX and elemental mapping

The details of the elemental analysis of the prepared materials PANI, PANI/AC, PANI/CuF, and PANI/AC/CuF have been shown in figure 6.4, showing the presence of all the expected elements. A slight increase of C % in the case of PANI/AC could be observed as compared to PANI, which may be due to the addition of AC. The composition of C was reduced in both the

composite materials PANI/CuF and PANI/AC/CuF as compared to PANI/AC. The deviation in the composition of N and O may be due to the addition of other elements in binary and ternary composite materials. Again, the lower composition of S may be attributed to the extensive washing of the samples during preparation. The presence of K could be observed due to the activation of AC with KOH. the atomic ratio of Cu and Fe is approximately 0.5, which is relatable from the chemical formula $CuFe_2O_4$. Similar pattern of change in composition of C, N, O and S was also observed on previously prepared composite materials PANI/AC/CuCo and PANI/AC/CoF.

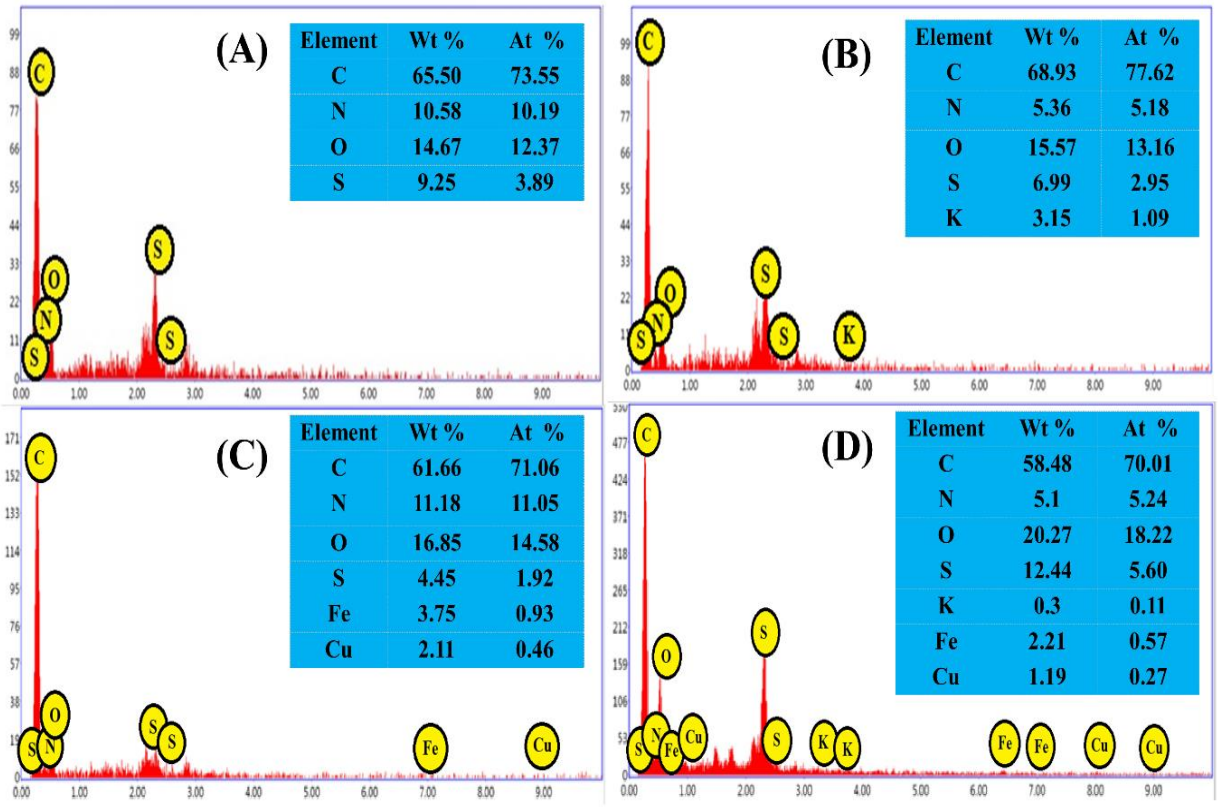

Fig 6.4: EDX analysis of (A) PANI, (B) PANI/AC, (C) PANI/CuF, and (D) PANI/AC/CuF

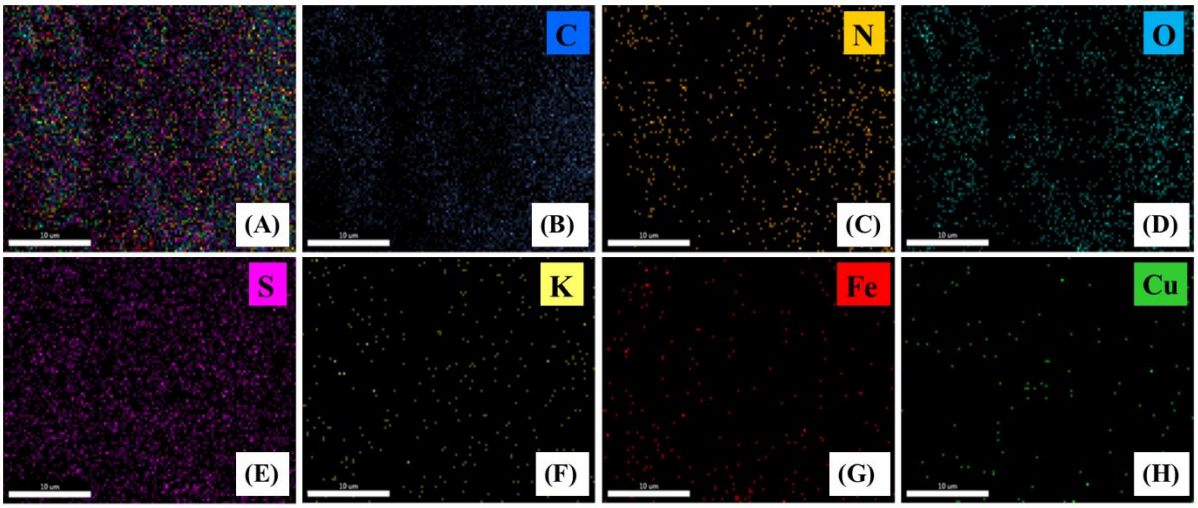

Fig 6.5: Elemental mapping of ternary composite material PANI/AC/CuF

The elemental mapping (combined and individual) of the ternary composite material PANI/AC/CuF has been demonstrated in figure 6.5, showing the uniform distribution of the expected elements. Also, it could be confirmed from the elemental mapping that the composition of C, N, O, and S is higher as compared to Cu, Fe, and K in the ternary composite PANI/AC/CuF.

6.2.5 X-ray photoelectron spectroscopy

The surface composition of the synthesized nanomaterials was confirmed by X-ray photoelectron spectroscopy. Figure 6.6 (A) shows the survey scan of pristine PANI, PANI/AC, PANI/CuF, and ternary PANI/AC/CuF, indicating the presence of C, N, O, and S in all the prepared samples. Also, the less intense peaks indicate the presence of Cu and Fe in the binary PANI/CuF and ternary PANI/AC/CuF materials. The high-resolution fitted spectrum of PANI/AC (Fig. A4 in appendix) demonstrated four different peaks at 284.51 eV, 285.51 eV, 286.92 eV, and 290.71, respectively. These peaks were attributed to (C-C) & (C=C), (C-O), (C=O) groups and π-π* "shake-up" satellite band due to the presence of AC, respectively.

Further, figure 6.6 (B) to (F) manifests different high-resolution spectra for ternary composite PANI/AC/CuF.

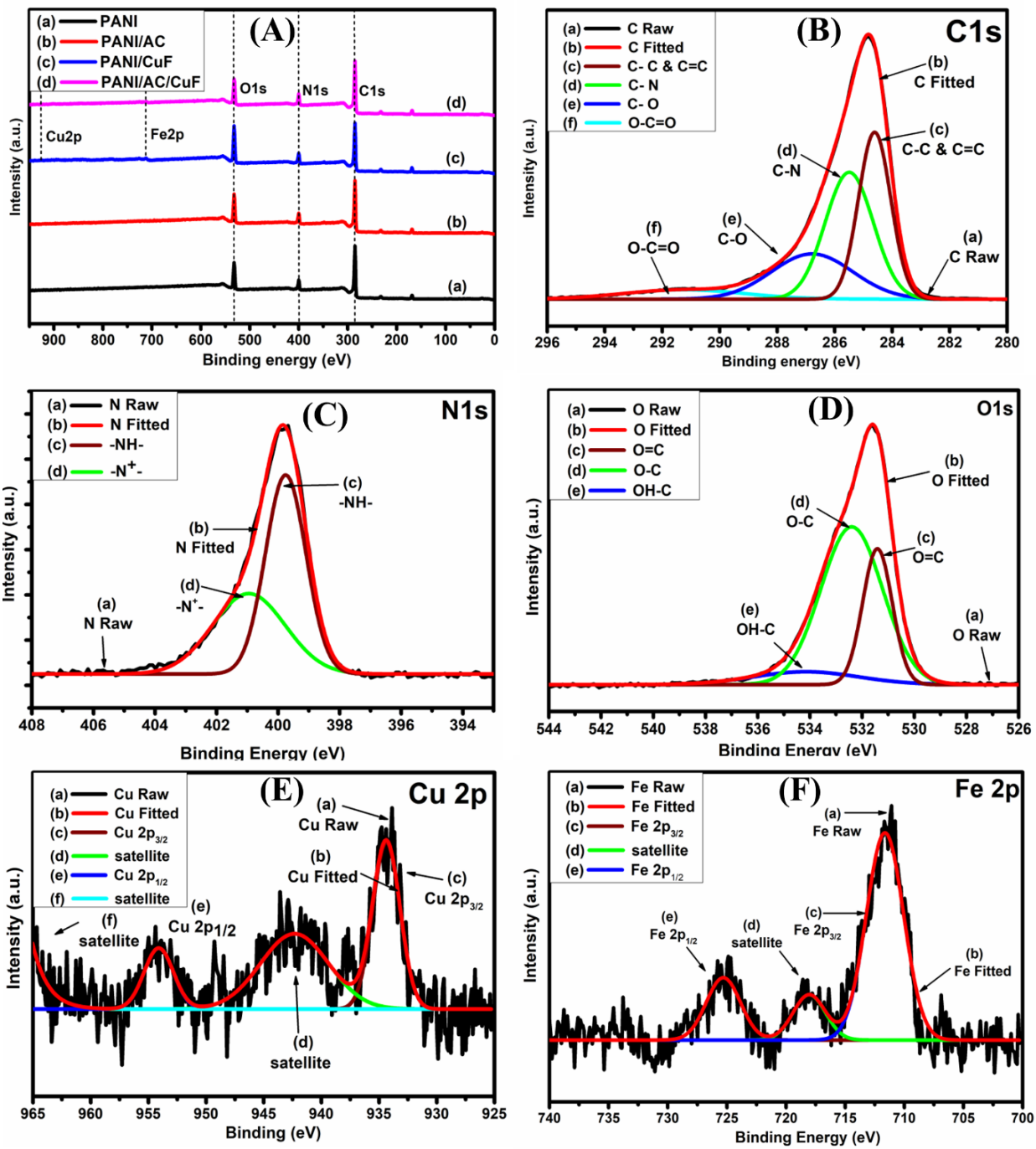

Fig 6.6: (A) XPS survey scan of PANI, PANI/AC, PANI/CuF, PANI/AC/CuF, (B) to (F) high-resolution spectra for C1s, N1s, O1s, Cu2p and Fe2p, respectively.

In the case of ternary PANI/AC/CuF, C1s high-resolution spectra (Figure 6.6 (B)) revealed four distinct peaks. The (C-C) & (C=C) were assigned for binding energy 284.61 eV. The (C-N) group was attributed to 285.49 eV. The (C-O) in alkoxy/epoxy was assigned to 286.79 eV,

and the (O-C=O) group with 291.24 eV, respectively. The N1s spectra (Figure 6.6 (C)) showed two peaks at 399.73 and 400.96 eV that were attributed to N cationic radical and benzoid amine (-NH-), respectively. The presence of conducting form of PANI was confirmed by these two peaks [239]. The O1s spectra (Figure 6.6 (D)) resolved into three distinctive peaks. The peak at 531.40 eV was present due to (C=O) from aromatic carbon, the peak at binding energy 532.41 eV was attributed to a carbon-oxygen single-bond group (C-O), and that at 534.19 eV was due to (C-OH) group (carbon-hydroxyl) [240,241].

Also, the two sharp peaks at 934.41 and 954.13 eV were present due to Cu $2p_{3/2}$ and Cu $2p_{1/2}$ with their respective satellite peaks at 942.26 and 964.9 as shown in figure 6.6 (E) [240]. These peaks confirm the presence of Cu in the ternary composite. The Fe spectra (Figure 6.6 (F)) in ternary composite PANI/AC/CuF deconvoluted into two strong characteristic peaks and one satellite peak. A sharp peak indicated the presence of Fe 2p3/2 binding energy 711.59 eV and its satellite peak at 718.00 eV [250]. Further, the peak at 725.3 eV corresponds to the presence of Fe $2p_{1/2}$ [242,243].

6.3 Electrochemical Characterizations

The 3E CV tests for prepared samples were conducted at 1 mVs^{-1}, as shown in figure 6.7 (A). The oxidation peaks of pristine PANI were observed at 0.28, 0.59, and 0.72 V, with corresponding reduction peaks at 0.03, 0.41, and 0.62 V. The transition from the leucoemeraldine to the emeraldine state was attributed to the peak at 0.28 V. The peak at 0.59 V was caused by hydroquinone/benzoquinone degradation. The peak at 0.72 V was associated with a transition from the emeraldine state to the pernigraniline state [251,252]. The different redox states of PANI has been presented in figure A.6 (appendix). The specific capacitance exhibited by pristine PANI was 388.7 Fg^{-1}. The binary PANI/AC, PANI/CuF, and ternary PANI/AC/CuF did not exhibit the PANI peak at 0.59 V, which may have been caused by the

inclusion of AC and $CuFe_2O_4$ particles. The CV of PANI/AC exhibited oxidation peaks at 0.2 V / 0.69 V and reduction peaks at 0.52/ 0.28 V, respectively. A combination of EDLC and pseudocapacitance, along with a larger voltammetric area than pure PANI, was obtained, indicating its better specific capacitance at 522.1 Fg^{-1}.

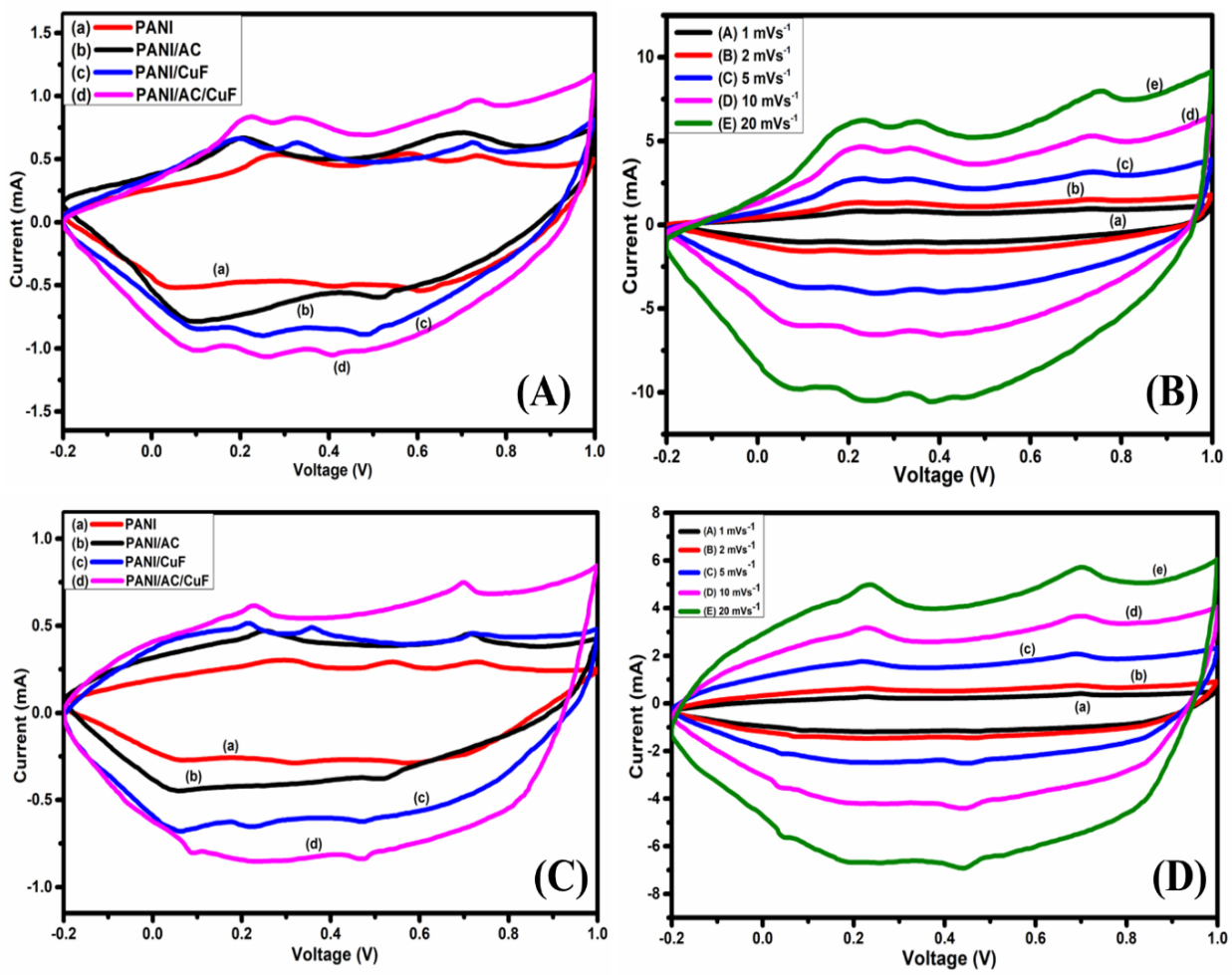

Fig 6.7: (A) 3E CV of prepared materials, (B) 3E CV of ternary PANI/AC/CuF at varying scan rates, (C) 2E CV of prepared materials, (D) 2E CV of ternary PANI/AC/CuF at varying scan rates

Furthermore, in the case of PANI/CuF, the oxidation peaks at 0.19 V, 0.32 V, and 0.72 V and corresponding reduction peaks at 0.48 V, 0.24 V, and 0.1 V corresponding to the combined effects of PANI, Cu^{2+}/ Cu^{3+}, and Fe^{2+}/ Fe^{3+} transitions. A redox reaction mechanism of

$CuFe_2O_4$ has been presented in appendix (eq. C). The binary PANI/CuF demonstrated a specific capacitance of 631.3 Fg^{-1}. The observed oxidation peaks occurred at 0.21 V, 0.32 V and 0.73 V and the corresponding reduction peaks were present at 0.10 V, 0.25 V and 0.40 V. The benzoquinone/hydroquinone transition peak is not present on the ternary composite which may be due to interactions of AC and CuF particles. The oxidation peak present at 0.73 V may either be due to emeraldine/pernigraniline or Fe^{2+}/Fe^{3+} transitions as both occur at similar potentials. The voltammetric area under curves is highest for PANI/AC/CuF-based ternary material with higher peak current values with 759.8 Fg^{-1} of specific capacitance. The probable reason for highest specific capacitance of PANI/AC/CuF as compared to PANI/AC/CuCo and PANI/AC/CoF may be the lowest crystalline size of CuF nanoparticles. The lower size of crystals of CuF offers greater dislocation density and grain boundary and eventually more sites for electrochemical reactions [260]. Multiple scan rates of 2, 5, 10, and 20 mVs^{-1} were used to study the behavior of ternary nanocomposite PANI/AC/CuF (Figure 6.7 (B)), which manifested specific capacitance of 628.4, 534.3, 456.9, and 369.7 Fg^{-1}, respectively. The peak current responses rise with the increase in scan rate, implying rapid charge propagation. With the rise in voltammetric scan rates, the area under the CV curves rises, showing the ternary material is highly capacitive. Also, forward scan peaks were shifted to a slightly more positive direction, whereas reverse scan peaks moved to a slightly more negative direction, indicating the presence of strong capacitive and faradaic currents. For 2E symmetric configurations, the CV was performed at $1mVs^{-1}$, as demonstrated in (Figure 6.7 (C)). Again, the ternary nanocomposite PANI/AC/CuF exhibited the highest voltammetric area, indicating its high specific capacitance. The combination of EDLC and the pseudocapacitive nature of the materials may be responsible for high specific capacitance. Further, with the rise in voltammetric scan rates, the voltammetric area of CV curves increases figure 6.7 (D), which may be attributed to rising capacitive current at with increase in voltammetric scan rates. The

electrolyte ions, however, don't get sufficient time to travel to the active sites as scan speeds increase, which causes a decrease in specific capacitance. Therefore, it cannot reciprocate with corresponding reversible redox reactions compared to that at lower scan rates.

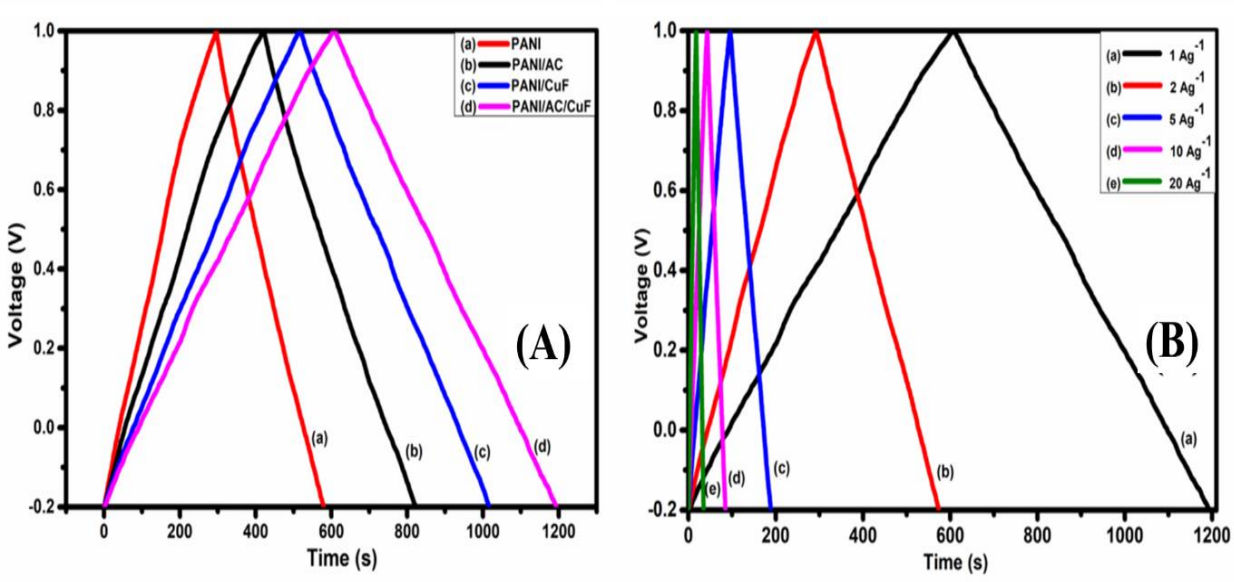

Fig 6.8: GCD characteristics of (A) PANI, PANI/AC, PANI/CuF and PANI/AC/CuF at 1 A/g, (B) ternary PANI/AC/CuF at varying current density from 1 A/g to 20 A/g.

The charging and discharging behavior of the fabricated electrodes has been presented in Figure 6.8 (A). The synthesized materials exhibited symmetrical triangular nature with few deviations or plateaus. The contribution of redox transitions, EDLC, and pseudocapacitive behavior may be the cause of these deviations. The highly linear and symmetric GCD profiles at all the different current densities imply excellent reversibility and good rate capability of the electrodes. A variation of current densities from 1 to 20 Ag^{-1} for PANI/AC/CuF was also performed, as shown in figure 6.8 (B). The charge-discharge plots of PANI/AC/CuF kept their symmetrical triangular nature intact, with rising values of current density up to 20 Ag^{-1}. Further, at higher current densities, the charging and discharging times are reduced drastically, which may be due to the inaccessibility to certain packets by ions at higher currents. These inactive sites pose an ion diffusion barrier for the electrolyte ions.

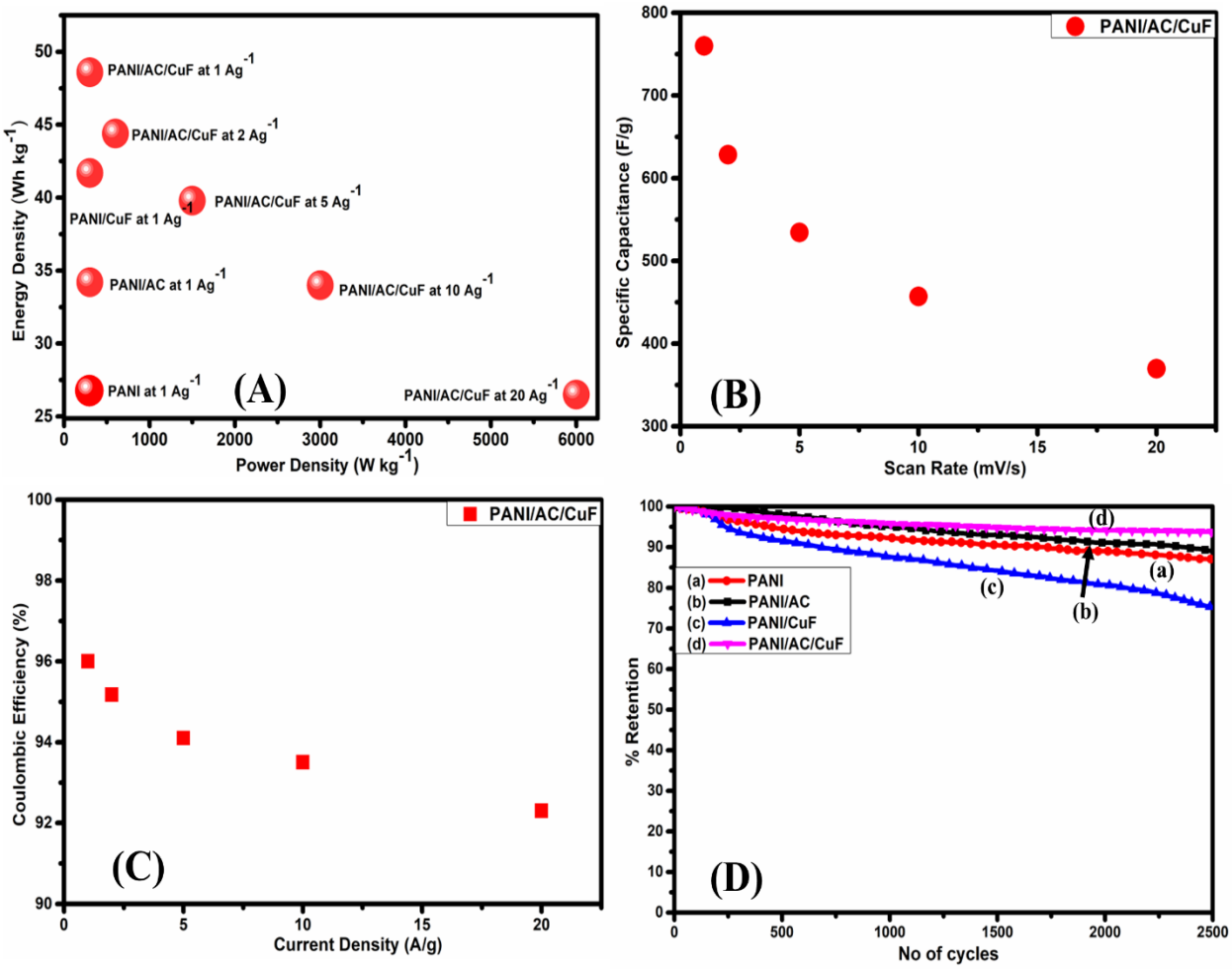

Fig. 6.9: (A) Ragone plot, (B) specific capacitance values at different values of voltammetric scan rates, (c) current density vs. coulombic efficiency, (D) Capacitance retention curves for the prepared samples

The Ragone plots for the prepared samples have been presented in figure 6.9 (A); it could be observed that ternary composite PANI/AC/CuF exhibited the highest specific energy compared to PANI/AC, PANI/CuF, and PANI. Table 6.1 demonstrates the values of specific capacitance, specific energy density, and power density for different synthesized materials. The higher energy density of ternary composite PANI/AC/CuF corresponds to its higher value of specific capacitance as compared to previously prepared PANI/AC/CuCo and PANI/AC/CoF. The ternary composite exhibits more charge storage capacity than other materials, as indicated by the specific power density. Fig 6.9 (B) demonstrates the change of specific capacitance with a

change in voltammetric scan rates. It was noted that the specific capacitance decreases with a rise in the value of the scan rate.

Table 6.1: The values of specific capacitance (C_{SP}), specific energy (E_{SP}), and specific power density (P_{SP}) for different synthesized materials

Material	**Scan Rate (mV/s)**	**C_{SP} (CV 3-E)**	**Current Density (A/g)**	**Esp (Wh/kg)**	**Psp (W/kg)**
PANI	1	388.7	1	25.7	300.1
PANI/AC	1	522.1	1	34.6	300.0
PANI/CuF	1	631.3	1	41.6	299.7
PANI/AC/CuF	1	759.8	1	49.6	300.0
PANI/AC/CuF	2	628.4	2	47.3	599.2
PANI/AC/CuF	5	534.3	5	38.5	1498.7
PANI/AC/CuF	10	456.9	10	34.1	3003.4
PANI/AC/CuF	20	369.7	20	28.2	5996.6

The charge transfer capacity can be broadly measured using coulombic efficiency. According to GCD plots, it can be described as the ratio of the charging time and discharging time of an electrode. The variation of coulombic efficiency vs. current density has been depicted in figure 6.9 (C). As current density rises, the coulombic efficiency falls, probably because the material is more irreversible at these current densities. At 20 A/g, the ternary composite had astounding coulombic efficiency of 92.2%.

To examine the capacitance retention of the prepared electrodes, the cyclic stability tests for the symmetric device were also conducted for 2500 cycles at 100 mV/s, as provided in figure

6.9 (D). PANI/AC/CuF, the ternary composite, exhibited a capacitance retention of 92.8 %, much higher than PANI/CuF, PANI/AC, and pure PANI samples.

The impedance studies of the electrodes fabricated synthesized materials were conducted to study the equivalent series resistance (ESR) and charge transfer resistance (Rct). ESR represents the sum of all the components, such as electrode-electrolyte contact resistance, material resistance, and electrolyte solution resistance. The abscissa intercept in the high-frequency region reflects equivalent series resistance (ESR), and the semicircle represents charge transfer resistance (Rct). PANI/AC/CuF-based electrode demonstrated a low ESR of 1.5 Ω and Rct of 5.3 Ω. On the other hand, PANI/CuF, PANI/AC, and pure PANI showed ESR / Rct at 2.4 / 7.6 Ω, 1.4/7.9 Ω, and 1.5/ 7.6 Ω, respectively, as shown in figure 6.10 (A). These lower resistance values could cause the ternary nanocomposite PANI/AC/CuF's high capacitance retention characteristic and linear charge-discharge curve. The results confirm that substrate, current collector, and electrolyte offer low resistances and fast ion diffusion with rapid charge transfer with processes. The results illustrate that the electrolyte, substrate, and current collector provide low resistances, quick ion diffusion, and quick charge transfer processes.

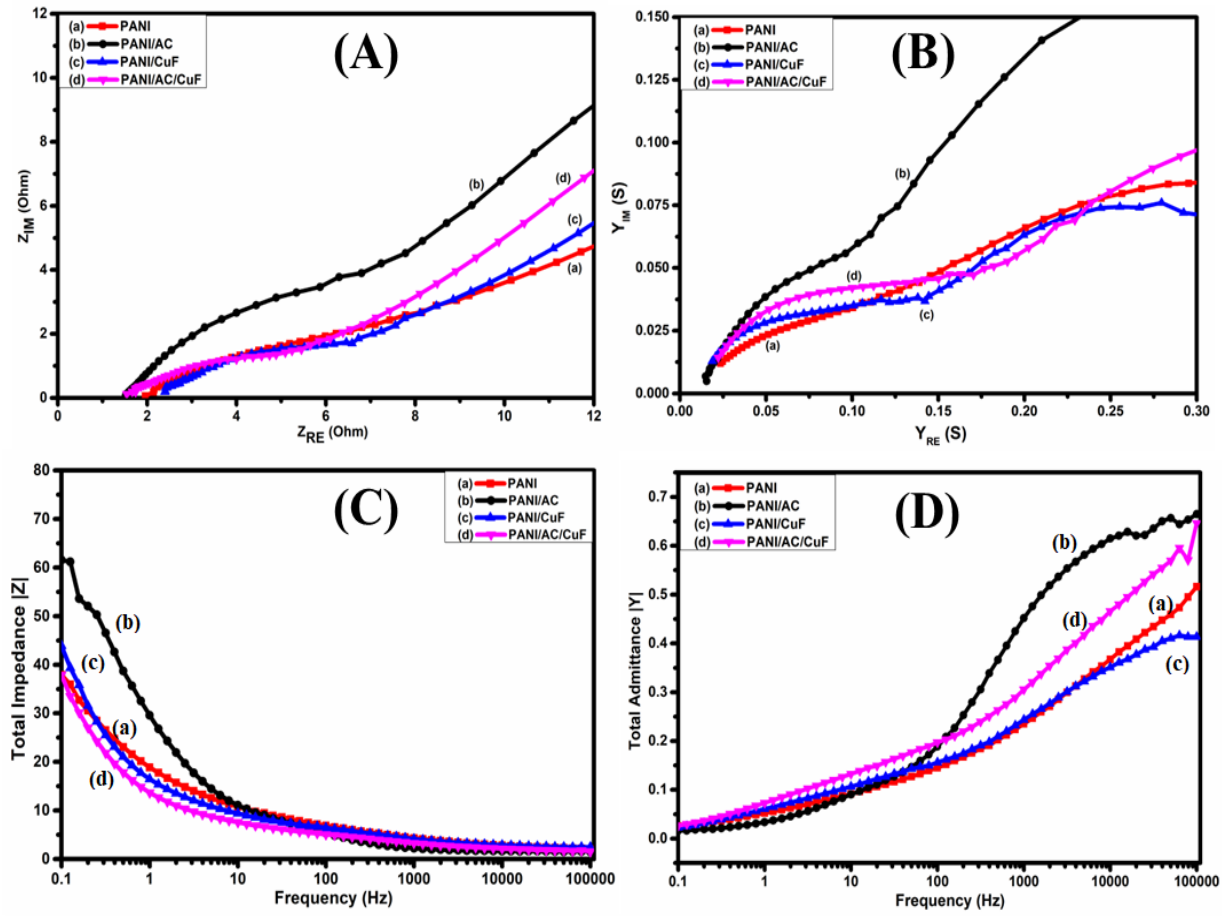

Fig 6.10: (A) Electrochemical impedance spectra (EIS) in the complex plane (B) Admittance plots in the complex plane. (C) normalized impedance |Z| vs. frequency, (D) normalized admittance vs. frequency

Frequency response investigations were conducted to assess the behavior of normalized admittance |Y|, impedance |Z|, capacitance |C|, and phase of Z as a function of frequency. Figure 6.10 (B) demonstrates the plot between real and imaginary components of total admittance |Y| for the prepared samples. Additionally, the relaxation time constant (t_r), which is the minimum time required to extract all supercapacitor energy with at least 50 % efficiency, is inversely related to knee frequency (f_k). The supercapacitor transitions between resistive and capacitive behavior at a frequency known as knee frequency. For ternary PANI/AC/CuF, PANI/CuF, PANI/AC, and PANI, the values of f_k obtained were 0.019, 0.025, 0.05, and 0.10 Hz, with corresponding response times (t_r) at 50.25, 40, 19.95 and 10 Hz, respectively.

Figure 6.10 (C) manifests normalized impedance |Z| vs. frequency for pure PANI, PANI/AC, PANI/CuF, and PANI/AC/CuF. The general trend is |Z| decreases with increased frequency for all the materials as impedance is reciprocal of admittance. The ternary composite PANI/AC/CuF exhibited the lowest value of impedance in the low-frequency regime. Figure 6.10 (D) represents the plot of normalized admittance |Y| with frequency for PANI, PANI/AC, PANI/CuF, and PANI/AC/CuF. For all of the prepared samples, it was observed that |Y| increases as the frequency increases as opposed to the impedance vs. frequency plot.

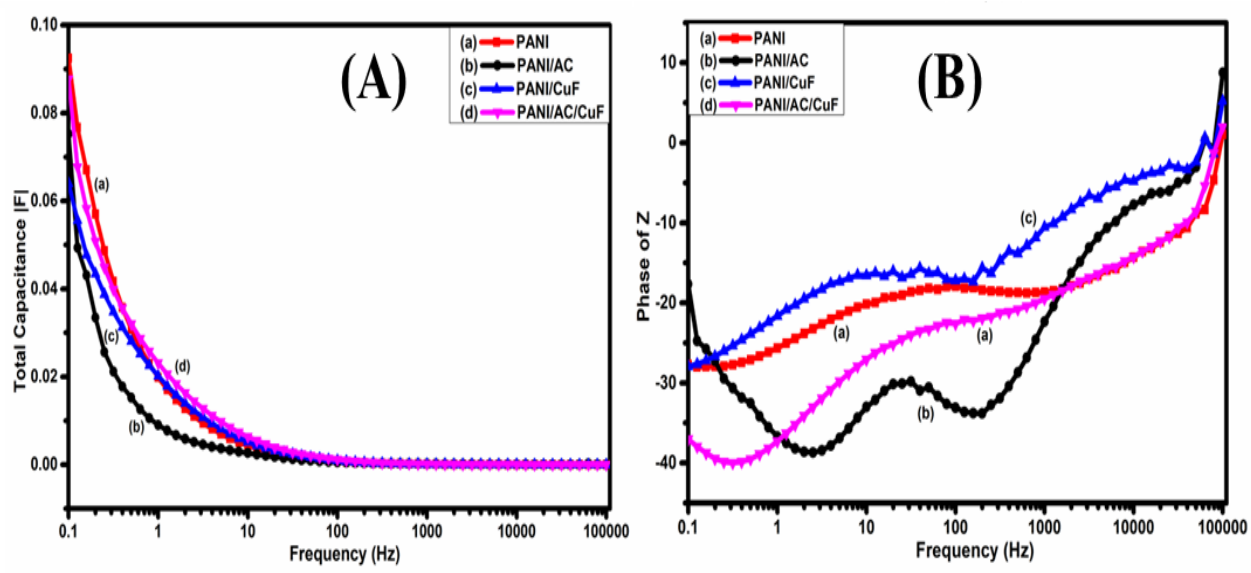

Fig. 6.11: (A) normalized capacitance |C| vs. freq, and (B) phase of |Z| (ϕ) vs. freq for the prepared samples.

Figure 6.11 (A) indicates the plot of normalized capacitance |C| vs. frequency. The normalized capacitance for all the materials declines with rising frequency, with PANI/AC/CuF exhibiting the best capacitance. These results further corroborated the nature of the prepared samples under various frequency levels and were obviously in good agreement with the EIS plot's results. The supercapacitors generally are resistive at high frequencies and capacitive at low frequencies [259]. The variation of phase of Z (ϕ) vs. frequency was also studied for the prepared samples, as presented in Figure 6.11 (B). For all the prepared samples, the phase of Z

remains negative for a greater part of the frequency band, exhibiting supercapacitive nature of electrodes. The phase angle is lagging at around 28° at low frequency for pristine PANI, representing its pseudocapacitive behaviour. For binary PANI/AC, due to the presence of AC, some EDLC behaviour was introduced, as evidenced by the rise in phase angle. The binary composite PANI/CuF in the low-frequency zone showed fluctuating and rising nature with frequency. For ternary composite, PANI/AC/CuF, a lag of 36° was observed in the low-frequency regime and which rises as the frequency increases.

6.4 Conclusion

A novel ternary composite material polyaniline-activated carbon-copper ferrite (PANI/AC/CuF) was synthesized and characterized with the help of XRD, FTIR, FESEM, EDX, and XPS. The EDLC behavior of activated carbon and the pseudocapacitive behavior of polyaniline and copper ferrite were responsible for the synergistic effects and excellent electrochemical activity of the ternary composite PANI/AC/CuF. Therefore, the ternary composite has been synthesized to take advantage of the individual components. The specific capacitance values of the ternary composite PANI/AC/CuF at 1 mVs^{-1} was 759.8 Fg^{-1}. The symmetric device based on PANI/AC/CuF demonstrated a high specific energy-density of 49.6 Wh/kg and a maximum specific power density of 5996.6 W/kg. The ternary composite PANI/AC/CuF resulted in 92.8 % of capacitance retention after 2500 cycles. This excellent stability may be due to activated carbon, which maintains the inherency of polyaniline and copper ferrite. EDLC behavior of activated carbon and the presence of redox-active sites in polyaniline and copper ferrite (pseudocapacitance) are responsible for the outstanding electrochemical property of the ternary composite PANI/AC/CuF. The lowest charge transfer resistance was exhibited by the ternary composite PANI/AC/CuF, which is also the material with the best cycle life. The ternary composite's superior properties make it a promising candidate for supercapacitor applications.

Part II: Optimization of polyaniline-based ternary composite material PANI/AC/CuF

In this part, ternary composite material PANI/AC/CuF was optimized by varying the weight percentage of AC and CuF and taking a fixed weight percentage of PANI using the response surface methodology for supercapacitor applications.

6.5 Central Composite design

The electrochemical properties of the prepared ternary composite material electrode are greatly influenced by the amount of AC and CuF used. It is essential to understand how their composition affects the electrochemical behavior in order to improve the specific capacitance value. Hence, optimization of composition of the composite is important. Response Surface Methodology (RSM) is amongst the most effective and extensively used techniques for optimization. The central composite design of RSM was utilized to optimize the weight percentage of AC (A) and weight percentage of CuF (B) in ternary composite with fixed weight percentage of PANI for electrochemical supercapacitor performance. This method offers a simple way to assess the interactions between various variables and only calls for a limited number of operations to optimize the response variable. Table 6.2 displays the experimental factor levels that were employed for optimization. The variables and their levels were chosen after a preliminary analysis, and the outcomes of basic experiments with 8 non-center points and 5 center points can be evaluated from the below equation.

$$N = 2^n + 2n + n_c = 2^2 + 2*2 + 5 = 13 \quad (1)$$

Where N = Total number of experiments to be performed, n = Number of independent variables, n_c = Number of centered points.

Table 6.2: Level of activated carbon (AC) and copper ferrite (CuF) for central composite design.

Variable	Name	Unit	Low value	High value
A (Numeric)	AC	weight percentage	1	5
B (Numeric)	CuF	weight percentage	1	5

6.6 Result and discussion

6.6.1 Optimization of ternary composite material based on RSM

13 groups of RSM experiments were produced after the experimental conditions for two influencing factors using design-expert software. A three-electrode configuration of CV tests was used to unify the experimental results in order to investigate the electrochemical performance of ternary PANI/AC/CuF based electrode. The specific capacitance determined from the CV curve at the scan rate of 1 mV/s incorporated the experimental results. Table 6.3 displays the final experimental results. Regression analysis used to fit the experimental data yields the second-order polynomial equation mode shown below.

$$C\ (F/g) = +629.02 - 145.18\ A - 59.95\ B - 16.65\ AB + 41.54\ A^2 - 87.66\ B^2 \quad (2)$$

Table 6.3: The experimental data and response values obtained by central composite design.

Sample	Polyaniline (PANI) (Fixed wt%)	Activated Carbon (AC) (Wt %)	Cobalt ferrite (CoF) (Wt %)	Specific Capacitance (F/g)
1	4	1	3	816.9
2	4	5	3	528.4
3	4	3	3	620.2
4	4	3	3	632.7

5	4	3	3	620.5
6	4	3	3	640.7
7	4	5	1	501.8
8	4	5	5	370.6
9	4	1	5	695.2
10	4	3	3	626.8
11	4	3	5	461.5
12	4	3	1	625.4
13	4	1	1	759.8

Analysis of variance (ANOVA) was used to determine the significance of the fitted equation, as shown in Table 6.4. The F-test resulted in a high F-value of 134.03, which suggested that the model had adequate significance ($P < 0.0001$) based on the findings of the ANOVA. The probability of getting this "model F-value" incorrectly was less than 0.01%. Typically, the P-value was employed to evaluate the importance of model terms. The related model term was more significant, as evidenced by the lower P-value. A, B, A^2, and B^2 are significant model terms in this scenario. In other terms, the precise capacitance values were significantly influenced by these two variables.

Table 6.4: ANOVA Response surface quadratic model for specific capacitance.

Source	Sum of Squares	df	Mean Square	F-value	P-value
Model	1.706E+05	5	34115.97	134.03	<0.0001*
A-AC	1.265E+05	1	1.265E+05	496.86	<0.0001
B-CuCo	21564.02	1	21564.02	84.72	<0.0001

AB	1108.89	1	1108.89	4.36	0.0753
A^2	4765.79	1	4765.79	18.72	0.0035
B^2	21223.40	1	21223.40	83.38	<0.0001
Residual	1781.77	7	254.54		
Cor Total	1.724E+05	12			

R^2 = 0.9897, R^2(Adjusted) = 0.9823, R^2(Predicted) = 0.9105, *Significant

The predicted R^2 of 0.9105 is in reasonable agreement with the adjusted R^2 of 0.9823; as the difference is less than 0.2.

The findings revealed an R^2 of 0.9897. The R^2 value measures the change in the model's average value, and the value of R^2 indicates how effectively the model can predict the experimental datasets. The model is highly relevant as a result. The R^2 (predicted) was 0.9105, with a difference of < 0.2 between it and the R^2 value. The experimental data from CV curves fitted the model's anticipated value quite well.

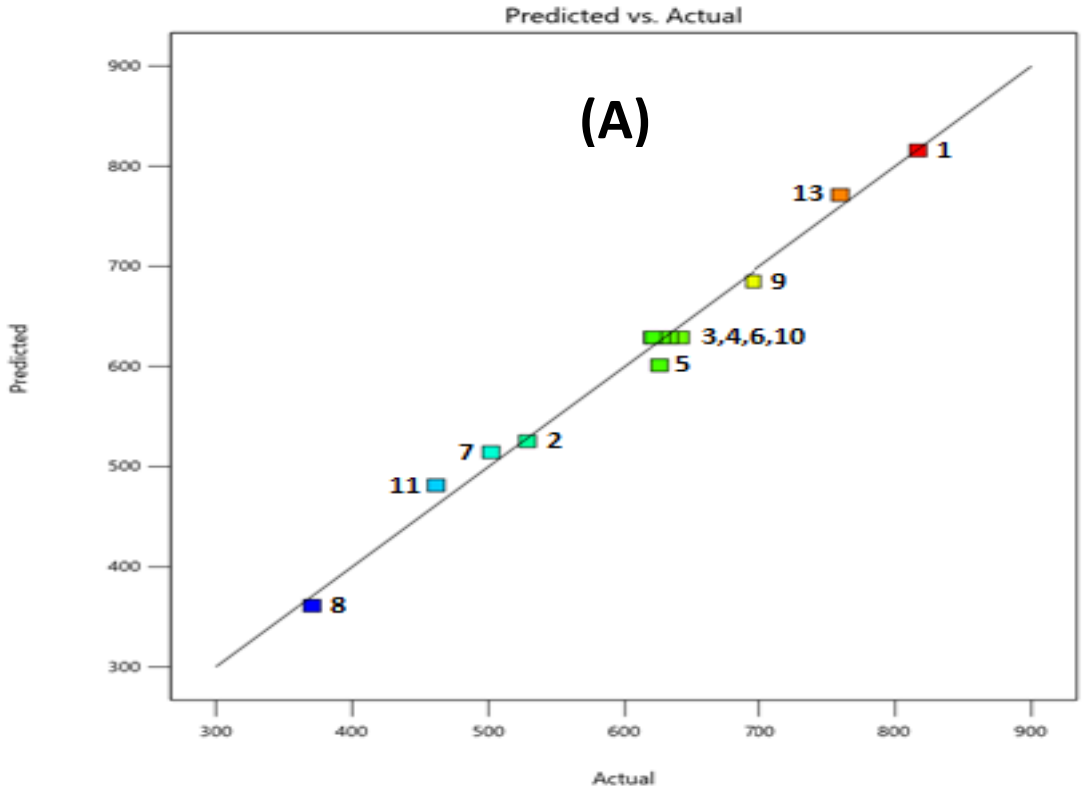

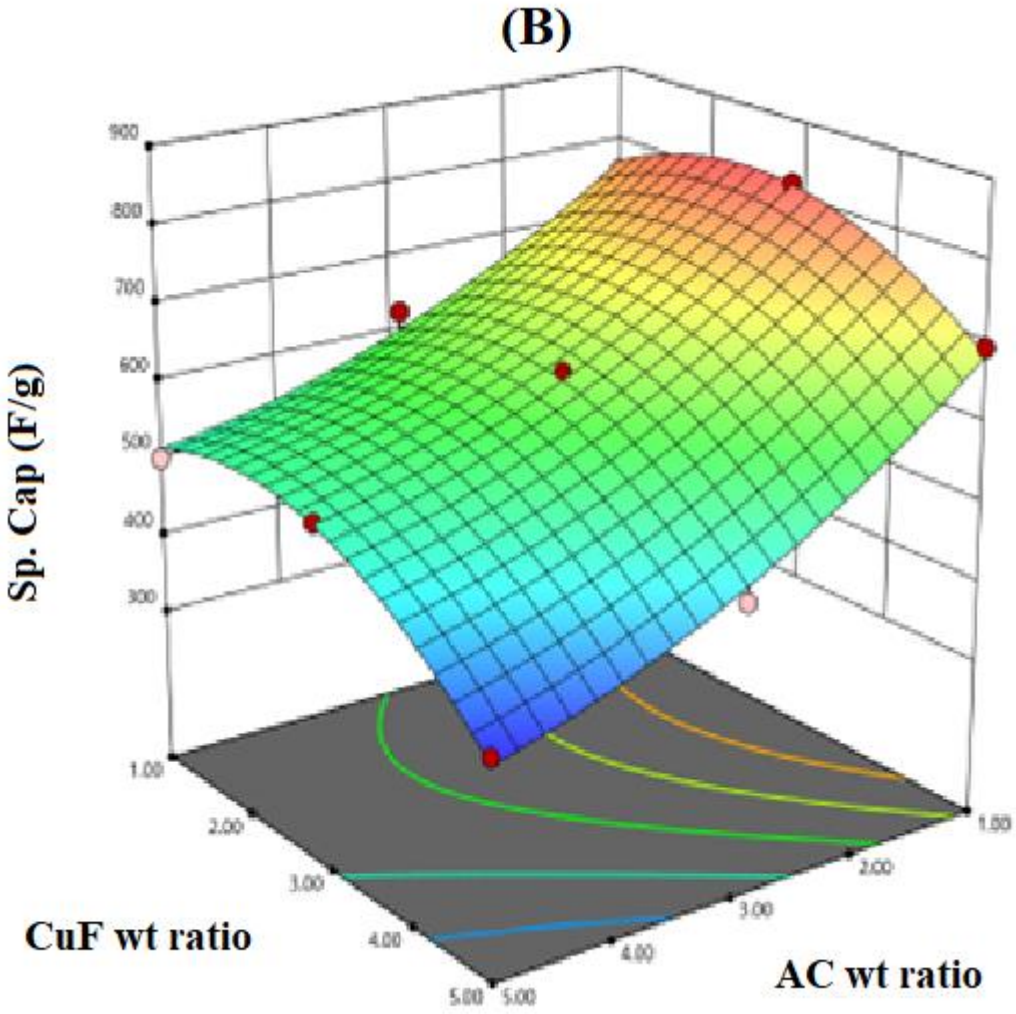
(B)
Sp. Cap (F/g)
900
800
700
600
500
400
300
CuF wt ratio
1.00
2.00
3.00
4.00
5.00
AC wt ratio
1.00
2.00
3.00
4.00
5.00

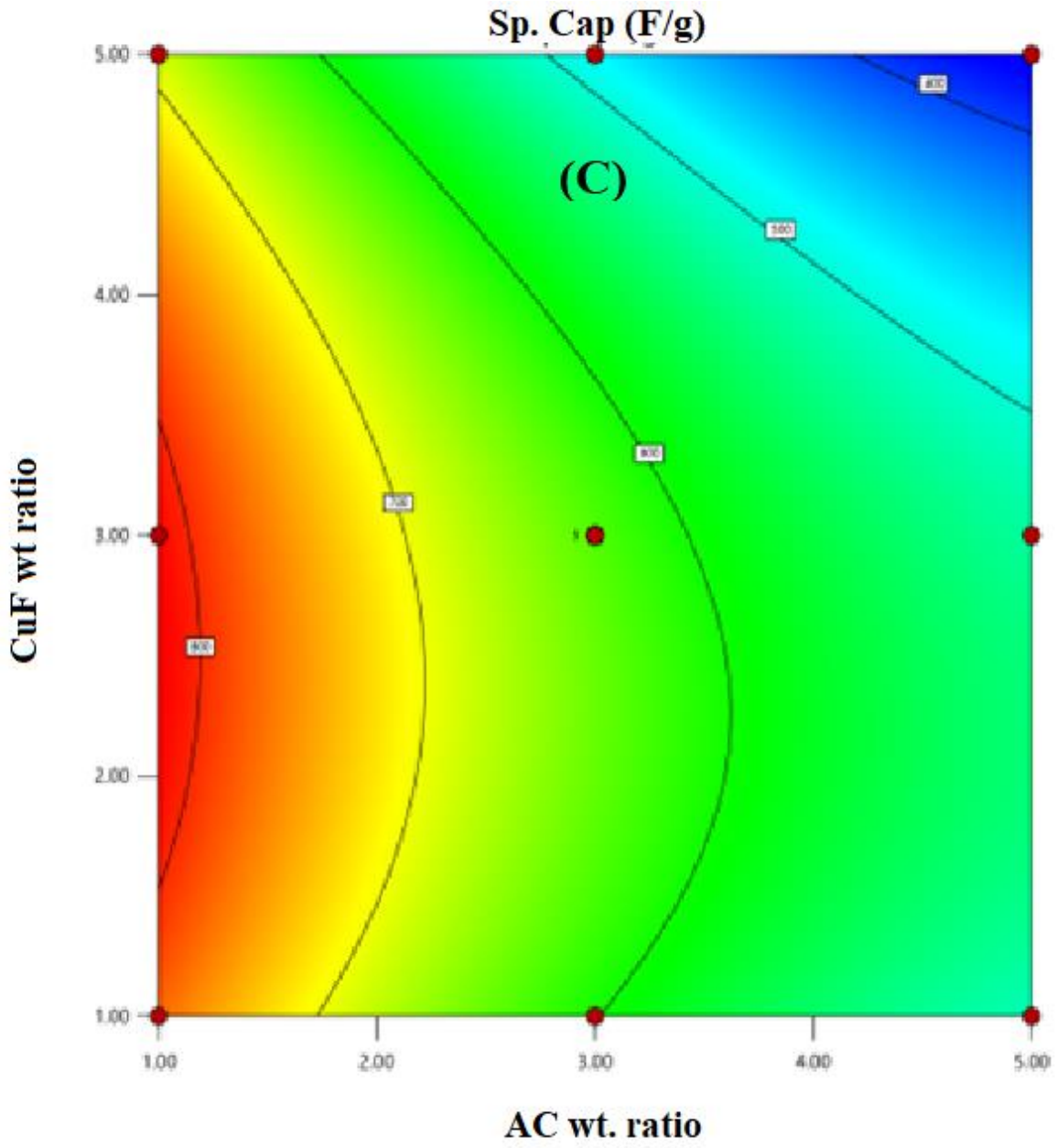

Fig. 6.12: (A) Predicted vs. actual response showing run numbers (B) 3D response surface curve, and (C) contour plot for AC (weight percentage) vs. CuF (weight percentage) as a function of specific capacitance

The primary function and relationship of independent variables can both be studied using the 3D (three-dimensional) response surface map. In order to further analyze the connection and optimum concentrations of the two components in raising specific capacitance, RSM was utilized. The predicted vs. actual response, 3D response surface curve, and contour plot have

been displayed in figure 6.12 (A), (B), and (C), respectively. The findings demonstrate that each variable has a maximum value and that the optimization criteria are consistent and obvious. In the 3D response plot, it can be observed that with the increasing weight percent of AC, the specific capacitance is decreasing. The reason behind the same may be that as activated carbon materials store charges by virtue of electrical double layer mechanism. However, the mechanism in pseudocapacitive materials i.e., conducting polymers and metal oxides is driven by oxidation reduction reactions. The combination of EDLC and pseudocapacitive materials (AC and CuF) exhibits better performance due to the synergistic effects of the individual components. Owing to electroststic adsorption, AC possess larger charge storage ability than CuF and too much porous surface is exposed to electrolyte ions for same amount of metal oxide particles. For this extra porous surface, there is no sufficient amount of metal oxide present and the contribution to specific capacitance comes largely from AC. Therefore, with an increase in carbon content, because of the reduced activity from the metal oxides (on increasing AC wt. percent,) the specific capacitance of the ternary composite material is decreasing.

According to the analysis of the response surface method, when the weight ratio of polyaniline, activated carbon, and copper ferrite in the ternary composite is in the ratio of 4:1:3 (PANI/AC/CuF), the maximum value of specific capacitance is 815.7 F/g. In summary, three parallel experiments were conducted to verify the model's reliability. The specific capacitance values of 813.1 F/g, 814.3 F/g, and 816.4 F/g were obtained with a mean value of 814.6 F/g, consistent with the predicted value of specific capacitance, showing that the proposed relationship model is highly accurate and reliable. This optimized ternary material PANI/AC/CuF was further considered for material and electrochemical investigations.

6.6.2 X-ray diffraction

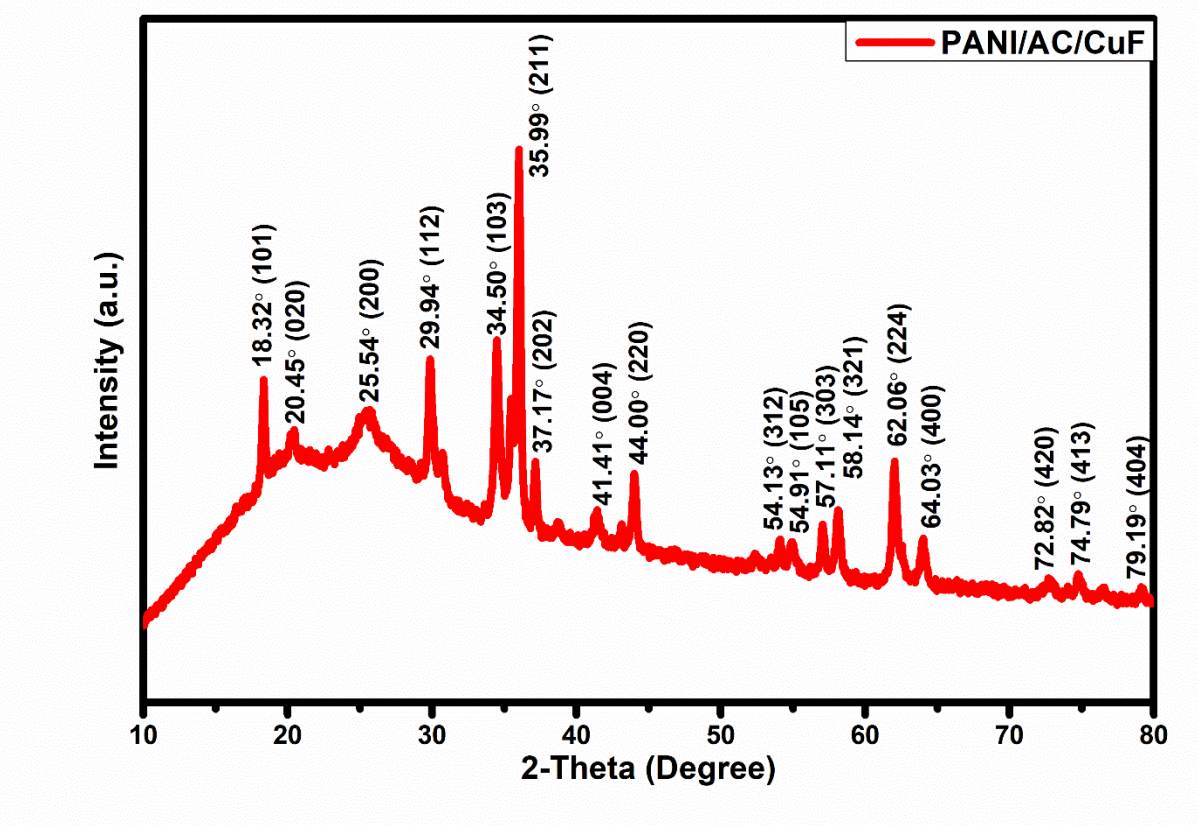

Fig. 6.13: XRD patterns of the optimized ternary composite PANI/AC/CuF

The XRD pattern of the optimized ternary composite material PANI/AC/CuF has been presented in figure 6.13. The characteristic diffraction peaks at 20.45° (020) and 25.54° (200) confirm the presence of polyaniline. The characteristic peak of AC could have been merged with the latter peak of PANI and, therefore, not visible individually. The peaks at 18.32° (101), 29.94° (112), 34.50° (103), 35.99° (211) 37.17° (202), 41.41° (004) 44.00° (220), 54.13° (312), 54.91° (105), 57.11° (303), 58.14° (321), 62.06° (224), 64.03° (400), 72.82° (420), 74.79° (413), and 79.19° (404) indicate the presence of copper ferrite in the optimized ternary composite material PANI/AC/CuF.

6.6.3 FTIR

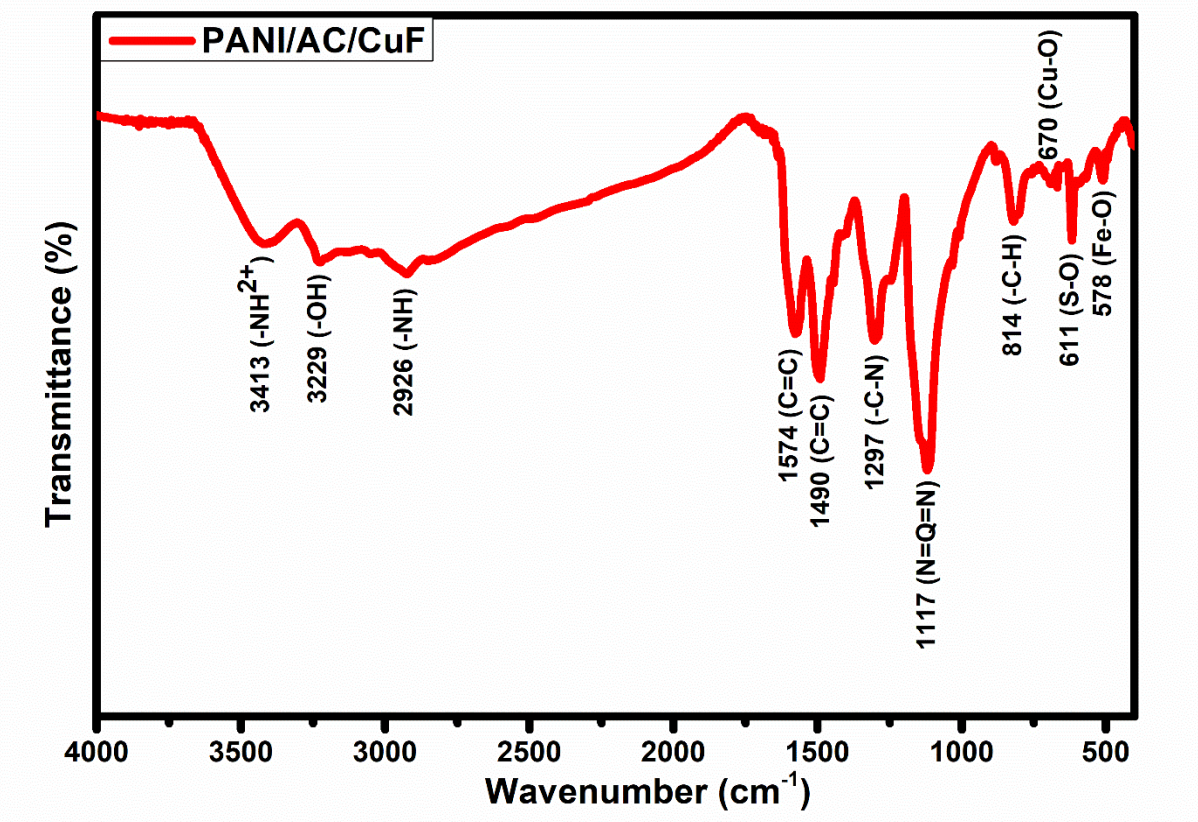

Fig. 6.14: FTIR spectra of the optimized ternary composite PANI/AC/CuF

The FTIR patterns of the optimized ternary composite material PANI/AC/CuF has been shown in figure 6.14. The absorption peaks at 3413 cm^{-1} and 3229 cm^{-1} are present due to $-NH^{2+}$ and -OH stretching. The band at 2926 cm^{-1} corresponds to -NH stretching vibrations. The absorption bands at 1574 cm^{-1} and 1490 cm^{-1} mark the C=C stretching vibrations in the quinoid and benzoid rings, respectively. Further, the more intense peak of benzoid rings indicates its presence in higher amounts as compared to the quinoid form. The -CN shuddering vibrations in the quinoid rings was associated with the absorption band at 1297 cm^{-1}. The p-substituted N=Q=N vibration was associated with the peak at 1117 $cm^{-1,}$ and -CH deformations due to the presence of PTSA in PANI were observed at the peak 814 cm^{-1}. The $-SO_3$ stretching vibrations due to the presence of PANI was present at 614 cm^{-1}. Further, the absorption bands at 670 cm^{-1} and 578 cm^{-1} were present due to Cu-O and Fe-O functional groups in the optimized ternary composite material PANI/AC/CuF.

6.6.4 Morphological analysis

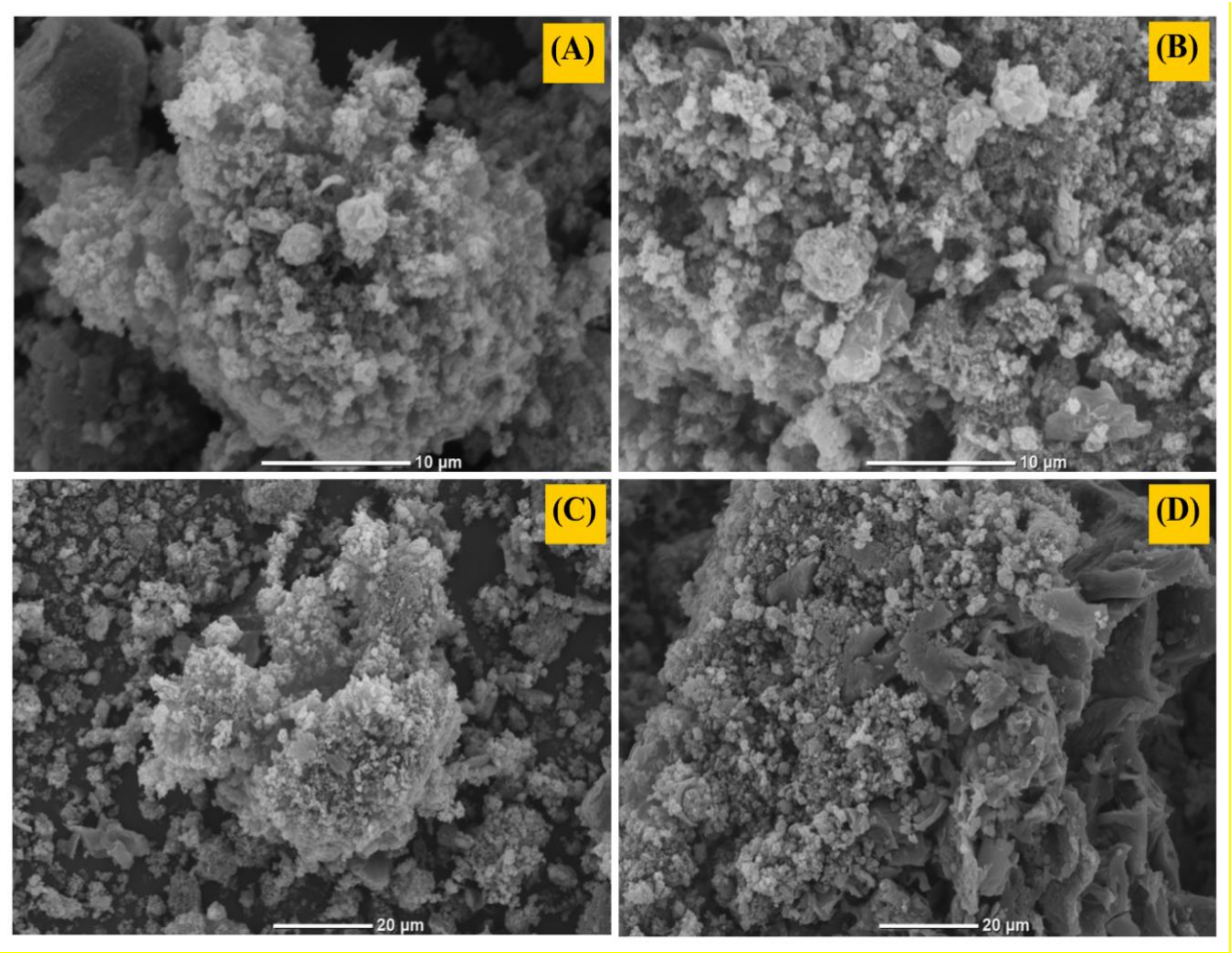

Fig. 6.15: SEM micrographs of the optimized ternary composite PANI/AC/CuF

The SEM micrographs of the optimized ternary composite PANI/AC/CuF have been provided in figure 6.15. Mostly, the texture of agglomeration could be observed in the SEM images. These micelle-like interconnected structures are responsible for the efficient transportation of charges. The large particle visible in figure 6.15 (D) is the porous activated carbon partially covered by PANI. In the other regions, it could be seen that the polyaniline have covered the activated carbon and copper ferrite particles.

6.6.5 EDX and Elemental Mapping:

The EDX spectrum of the optimized ternary composite PANI/AC/CuF has been provided in figure 6.16. The spectrum clearly shows the presence of all the expected elements. Figure 6.17 (combined and individual) shows the elemental mapping of the ternary composite material, indicating the uniform presence of all the expected elements.

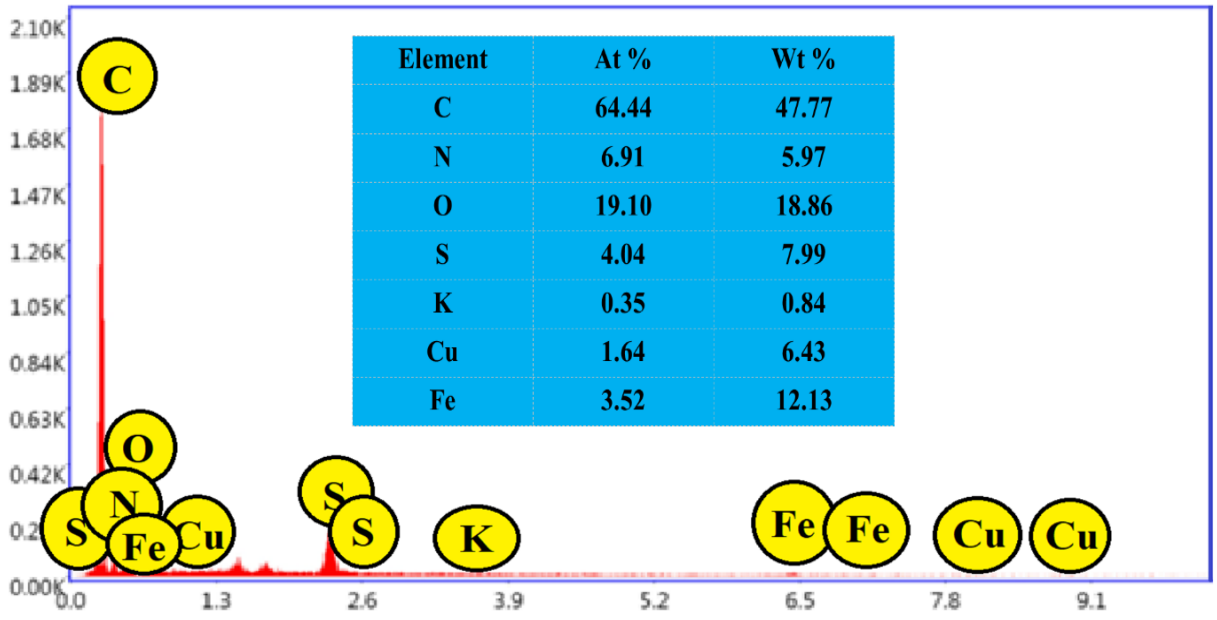

Element	At %	Wt %
C	64.44	47.77
N	6.91	5.97
O	19.10	18.86
S	4.04	7.99
K	0.35	0.84
Cu	1.64	6.43
Fe	3.52	12.13

Fig. 6. 16: EDX spectra for the optimized ternary composite PANI/AC/CuF

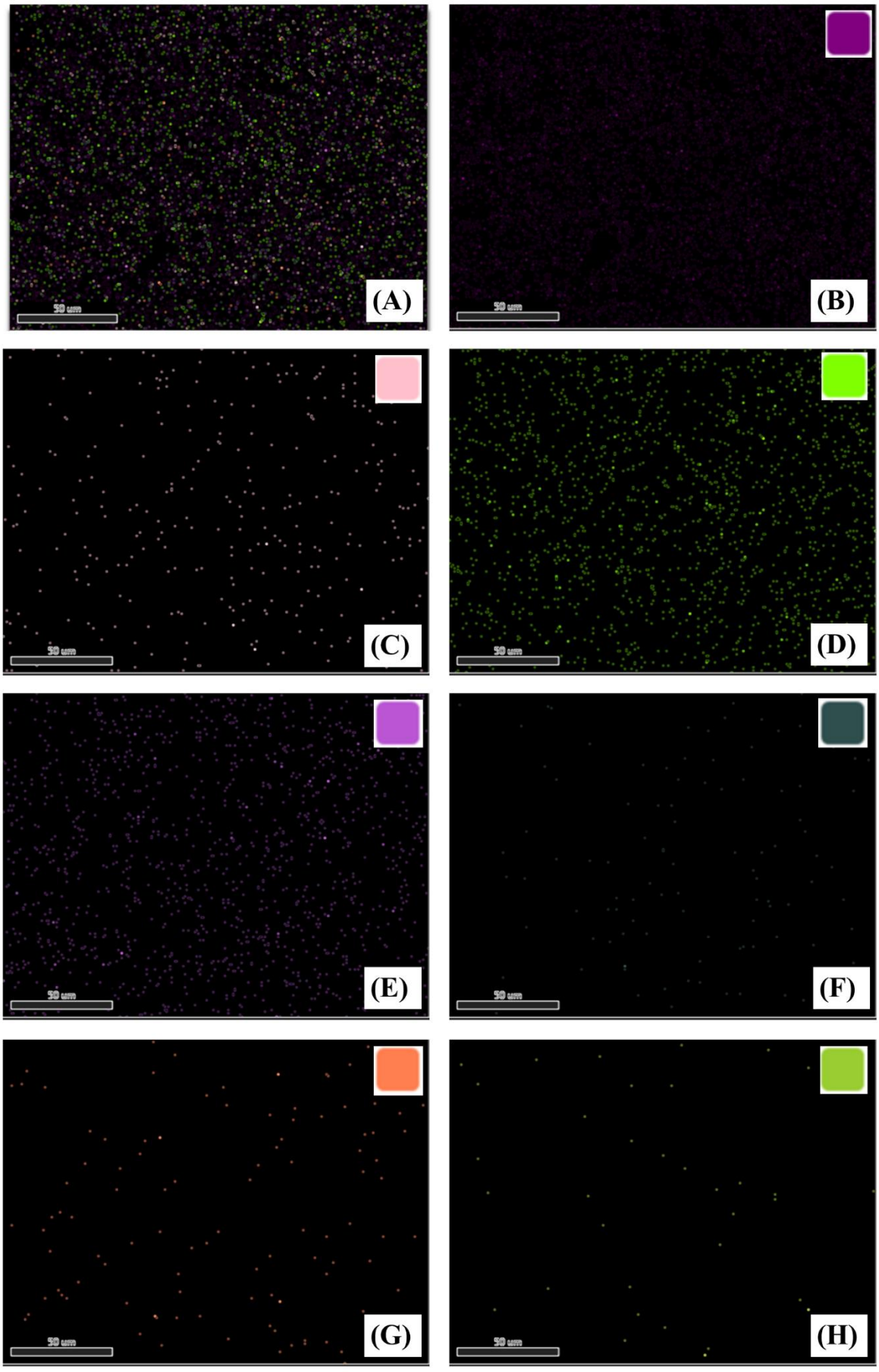
(A)
(B)
(C)
(D)
(E)
(F)
(G)
(H)

Fig. 6.17: Elemental mapping for the optimized ternary composite PANI/AC/CuF, showing (A) overlay, (B) carbon/ C, (C) nitrogen/ N, (D) oxygen/ O, (E) sulphur/ S, (F) potassium/ K, (G) iron/ Fe, (H) copper/ Cu elements

6.6.6 Electrochemical characterizations:

Cyclic voltammetry of the prepared electrode from the electrode prepared from optimized ternary composite PANI/AC/CuF was performed in 3-E and 2-E configurations, as shown in figure 6.16.

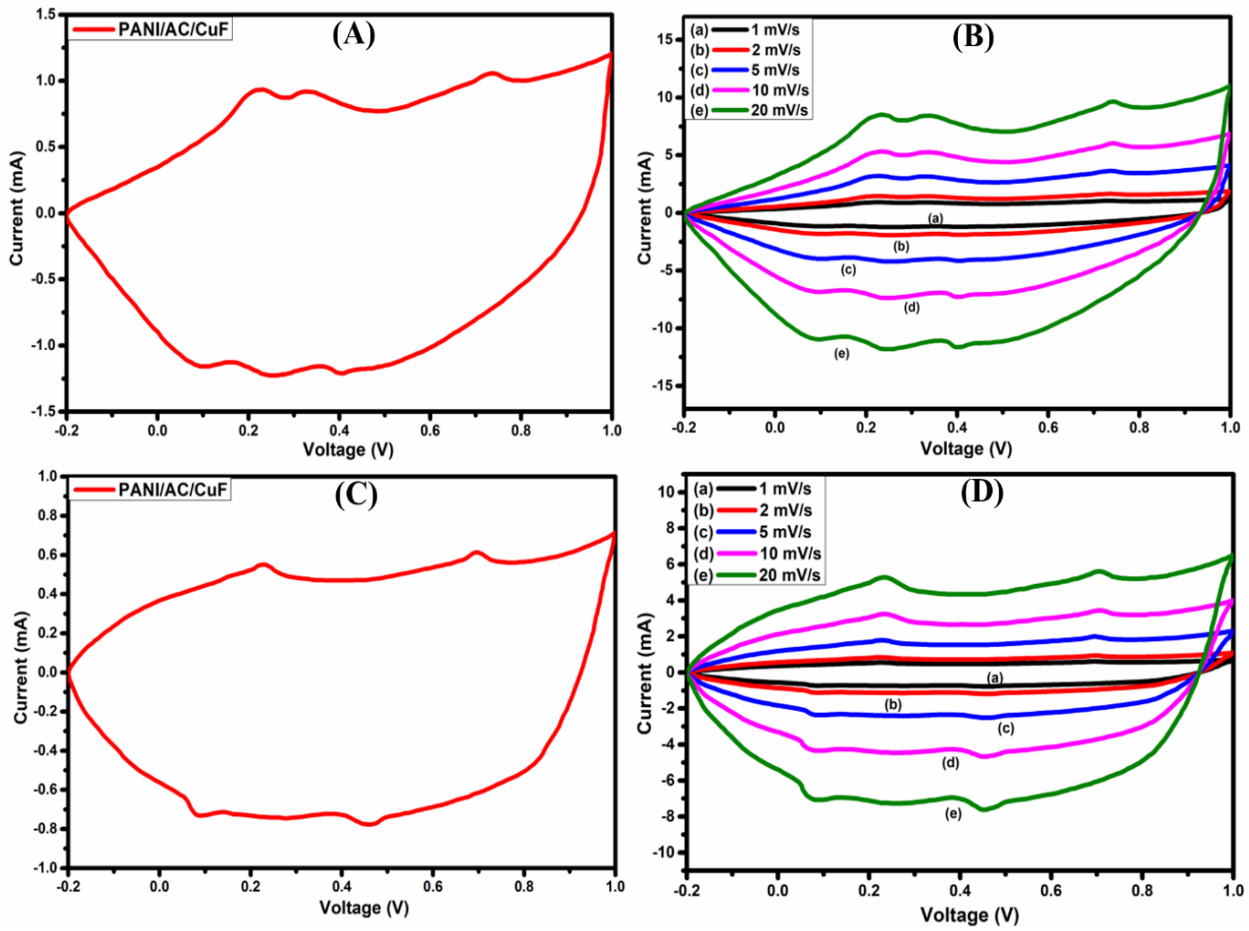

Fig 6.18: (A) 3E CV, (B) 3E CV at varying scan rates, (C) 2E CV, (D) 2E CV at varying scan rates for the optimized ternary composite PANI/AC/CuF

Figure 6.18 (A) demonstrates the 3-E cyclic voltammogram, where three oxidation peaks and three reduction peaks were observed in the forward scan and backward scan, respectively. The

specific capacitance value for the optimized ternary composite was PANI/AC/CuF at 1 mVs^{-1} was 816.4 Fg^{-1}. The ternary composite was also tested under varying voltammetric scan rates of 2, 5, 10, and 20 mVs^{-1} (Figure 6.18 (B)). The specific capacitance values for ternary PANI/AC/CuF at these scan rates were calculated as 641.1, 563.8, 482.5, and 387.9 Fg^{-1}. The area under the cyclic voltammetric curves increases successively with the scan rate, indicating a highly capacitive nature of the optimized ternary material PANI/AC/CuF. The shifting of the forward scan and backward scan peaks was minimal. The prepared electrodes were also evaluated under two-electrode symmetric configuration at 1 mVs^{-1} scan rate (Figure 6.18 (C)). The optimized ternary composite PANI/AC/CuF again demonstrated the highest voltammetric area and highest value of peak current. Further, the voltammetric area under the curves increases with the rise in scan rates to 2, 5, 10, and 20 mVs^{-1} (Figure 6.18 (D)).

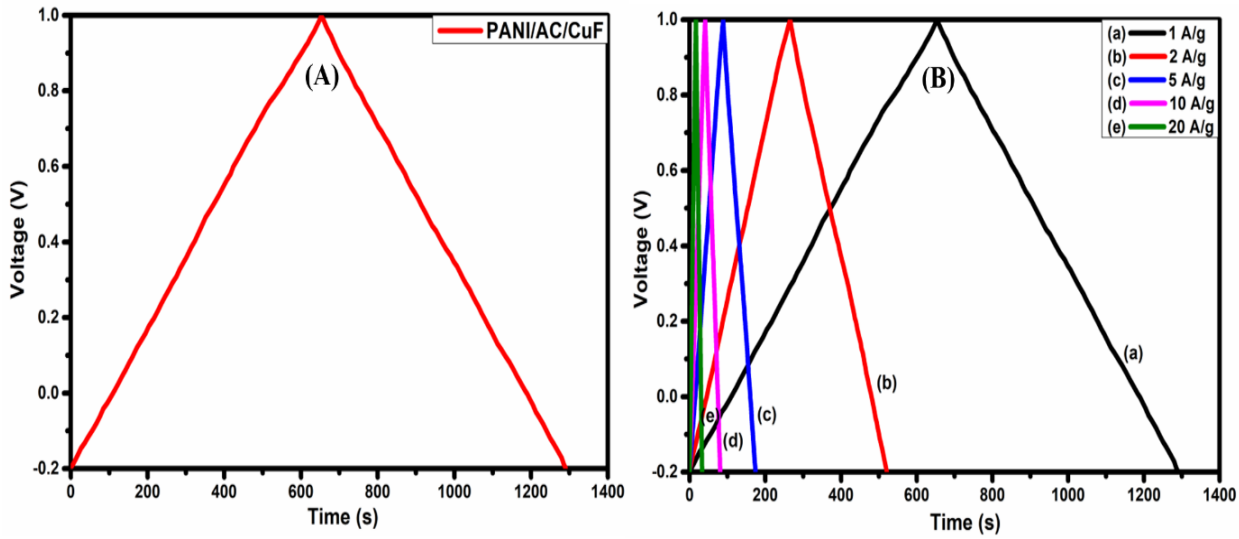

Fig 6.19: (A) 2E galvanostatic charge-discharge (B) 2E galvanostatic charge-discharge at varying current density for the optimized ternary composite PANI/AC/CuF

The galvanostatic charge-discharge tests were conducted for the optimized composite material-based electrodes under 2-E symmetric configuration. The charge-discharge plot at 1 Ag^{-1} current density has been presented in figure 6.19 (A), for which the specific capacitance was

found to be 265.1 Fg^{-1}. The material demonstrated a similar triangular behavior on the charge-discharge curve with minor plateaus, which may be attributed to the dual behavior (EDLC and pseudocapacitive). The optimized ternary composite PANI/AC/CuF was also evaluated under varying current densities of 2, 5, 10, and 20 $Ag^{-1,}$ as shown in figure 6.19 (B). With the rise in current density values, a sharp decline in the charging-discharging times was observed owing to the inaccessibility of electrolyte ions into the material.

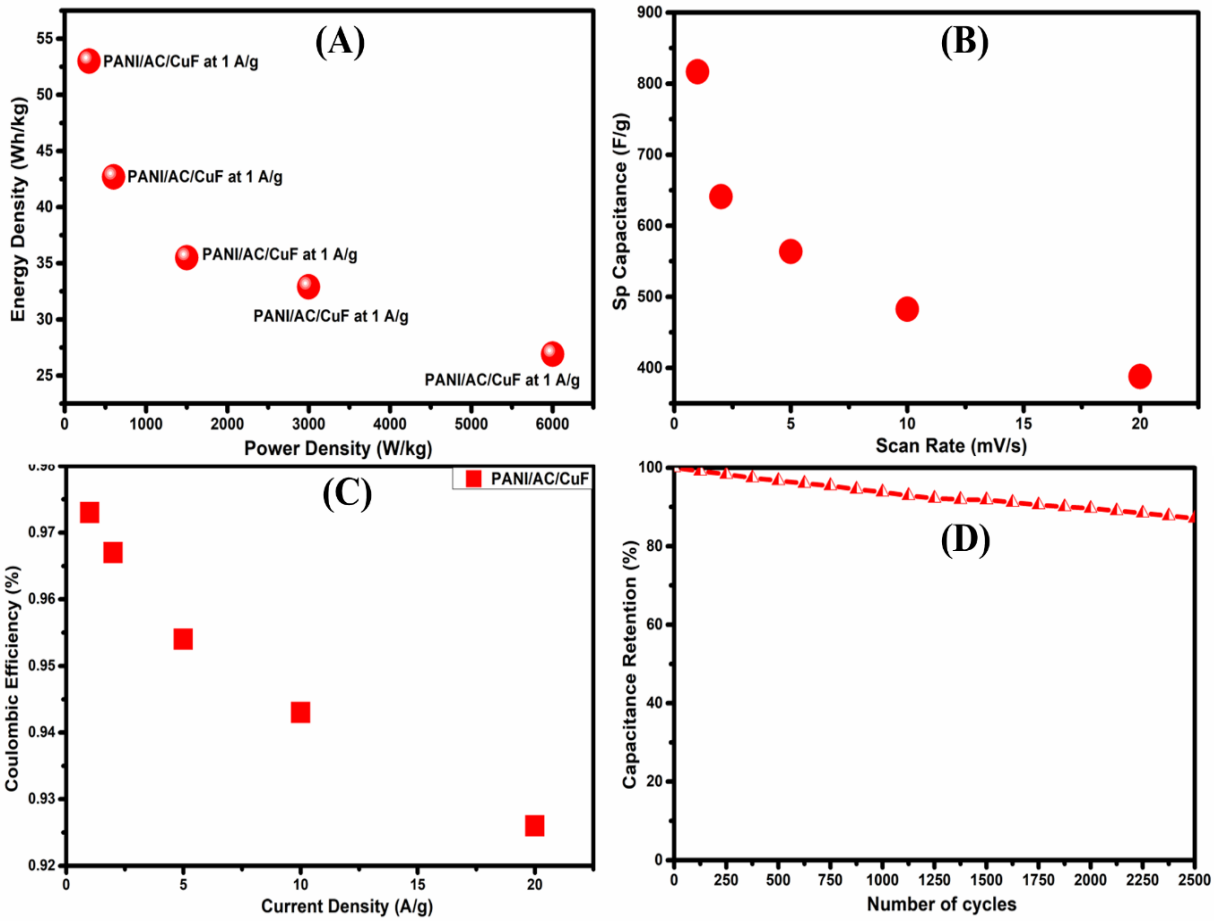

Fig 6.20. (A) Ragone plot, (B) 3E specific capacitance values at different values of voltammetric scan rates, (c) current density vs. coulombic efficiency, (D) Capacitance retention curve for the optimized ternary composite PANI/AC/CuF

Figure 6.20 (A) shows the Ragone plot for the optimized ternary composite PANI/AC/CuF. It was observed that at higher values of current density, the specific energy density declined,

whereas the specific power density increased. The peak specific energy density for the optimized ternary composite PANI/AC/CuF was 53.0 $Whkg^{-1}$ with 299.9 Wkg^{-1} of specific power density. The same ternary composite demonstrated the highest specific power density of 6000.1 W kg^{-1} with a specific energy density of 26.9 $Whkg^{-1}$ at 20 A/g. These high values of specific energy-density and specific power density correspond to the presence of both EDLC and pseudocapacitive materials in single composite material. Figure 6.20 (B) demonstrates the variation of measured values of 3- E specific capacitance with scan rate. Figure 6.20 (C) shows the variation of coulombic efficiency with current density, which decreases as current density increases. The capacitance retention tests for the 2E symmetric system were conducted to study the capacitance retention of the fabricated electrodes at a scan rate of 100 mV/s for 2500 cycles. The optimized ternary composite material PANI/AC/CuF showed outstanding capacitance retention of 87.1 % of the initial value (Figure 6.20 (D)). Table 6.5 shows the different values of specific capacitance, specific energy-density, and specific power-density for the optimized ternary material PANI/AC/CuF.

Table 6.5: The values of specific capacitance (C_{SP}), specific energy-density (E_{SP}), and specific power-density (P_{SP}) for optimized ternary composite PANI/AC/CuF.

Material	**Scan Rate (mV/s)**	**C_{SP} (CV 3-E)**	**Current Density (A/g)**	**Esp (Wh/kg)**	**Psp (W/kg)**
PANI/AC/CuF	1	816.4	1	53.0	299.9
PANI/AC/CuF	2	641.1	2	42.7	601.1
PANI/AC/CuF	5	563.8	5	35.5	1501.2
PANI/AC/CuF	10	482.5	10	32.9	2997.8
PANI/AC/CuF	20	387.9	20	26.9	6000.1

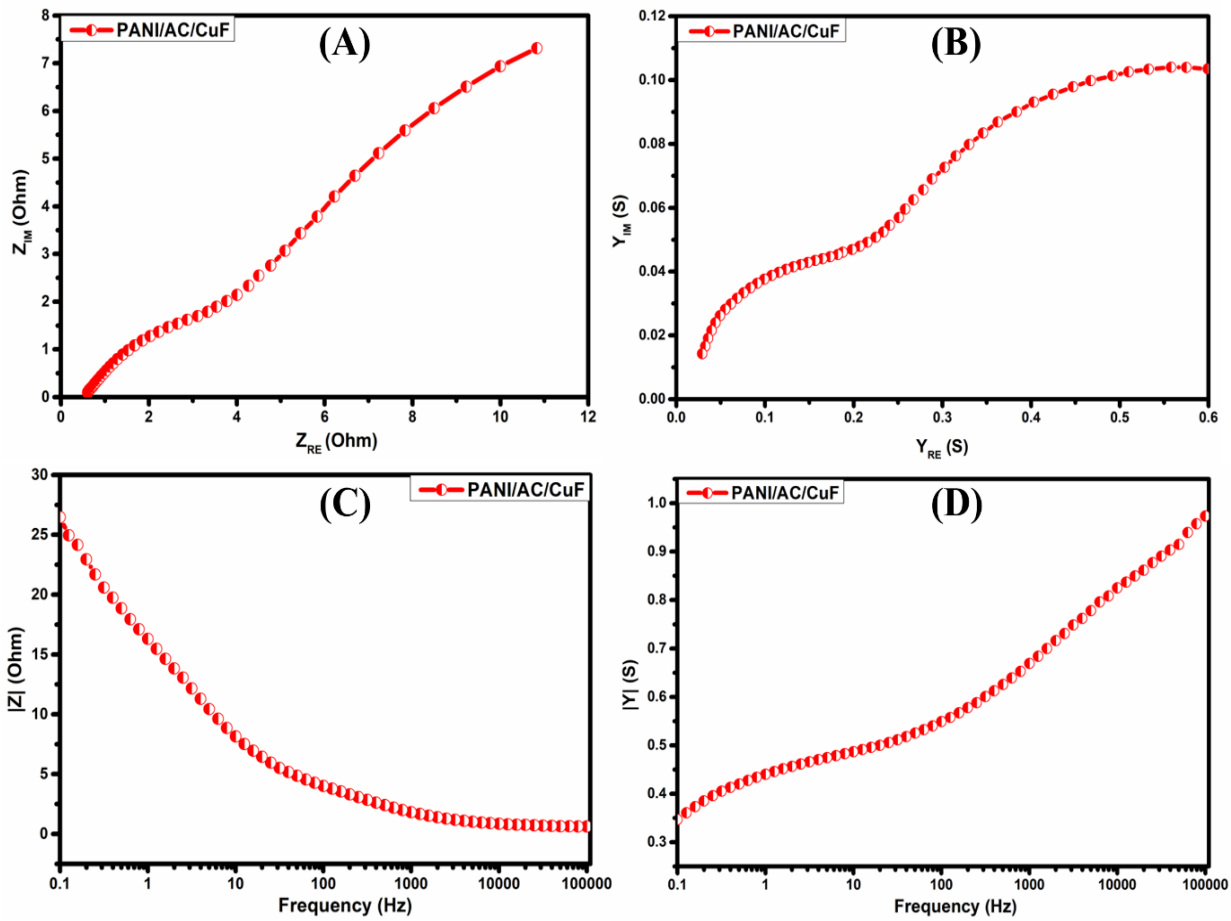

Fig 6.21: (A) Electrochemical impedance spectra (EIS) in the complex plane (B) Admittance plots in the complex plane. (C) normalized impedance |Z| vs. frequency, (D) normalized admittance |Y| vs. frequency for the optimized ternary composite PANI/AC/CuF

The impedance characteristics of the prepared electrodes from the optimized PANI/AC/CuF frequency response tests were conducted in the frequency range of 0.1 to 100000 Hz. The values of ESR (equivalent series resistance) and Rct (charge transfer resistance) were calculated as 0.68 Ω and 4.82 Ω, respectively, as shown in figure 6.21 (A). Further, the admittance properties of the fabricated electrodes were also studied in the form of Y_{RE} vs. Y_{IM} plots. Figure 6.21 (B) shows the variation of real admittance (Y_{RE}) vs. the imaginary admittance (Y_{IM}) for the fabricated electrode from optimized PANI/AC/CuF. Fig 6.21 (C) shows the

variation impedance |Z| with frequency. It was observed that |Z| decreases with a rise in frequency. Fig 6.21 (D) shows the variation of |Y| vs. frequency. It was noted that with the rise in frequency, |Y| increases as electrolyte ions vibrate faster at higher frequencies as opposed to |Z|.

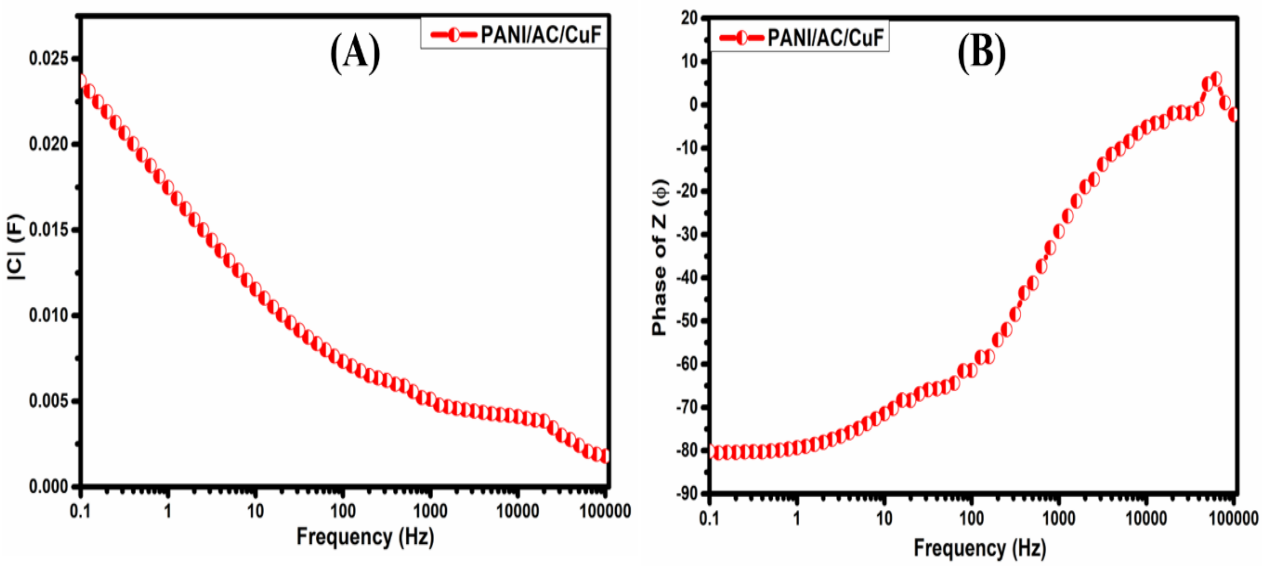

Fig 6.22: (A) normalized capacitance |C| vs. frequency, and (B) phase of |Z| (ϕ) vs. frequency of the optimized ternary composite PANI/AC/CuF

Figure 6.22 (A) shows the variation of normalized capacitance |C| with frequency. The value of total or normalized capacitance decreases as frequency increases, which is in good agreement with the previous EIS results. Figure 6.22 (B) shows the variation of the phase of Z (ϕ) with frequency for the optimized PANI/AC/CuF. The phase angle in the low-frequency regime is about 80°, indicating its highly pseudocapacitive nature.

6.7 Comparison of electrochemical performance of optimized ternary composite materials:

In the current section, a short comparison of electrochemical performance of optimized ternary composite materials has been discussed. For comparison, three-electrode cyclic voltammetric

curves of the optimized composite materials PANI/AC/CuCO, PANI/AC/CoF and PANI/AC/CuF have been plotted and presented in figure 6.23.

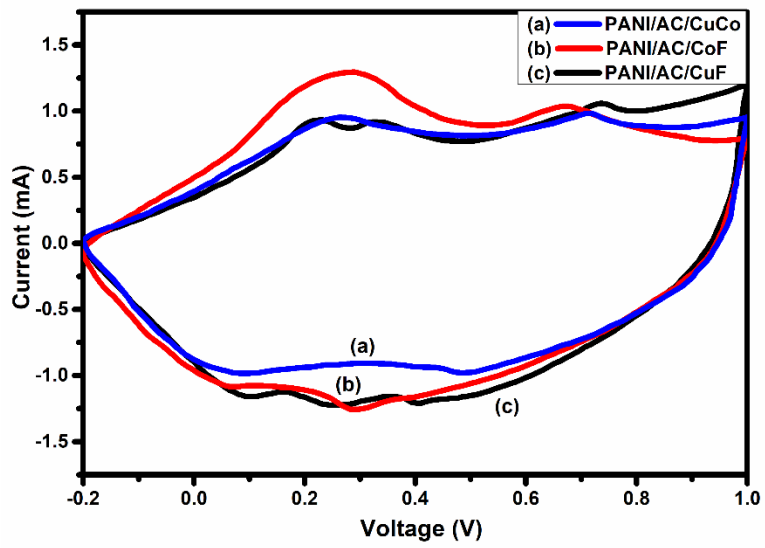

Fig 6.23: Comparison of CV curves for the optimized ternary composite materials PANI/AC/CuCo, PANI/AC/CoF, and PANI/AC/CuF.

The optimized composition for PANI/AC/CuCo was obtained as 4:1:3 (PANI:AC:CuCo) and corresponding specific capacitance was 694.8 F/g. In the case of ternary composite PANI/AC/CuCo, the peaks in the forward scan were located at 0.27/ 0.71 V, whereas those in the reverse scan were at 0.49/0.08 V, respectively. For PANI/AC/CoF, the optimized composition was obtained as 4:1.03:2.66 (PANI:AC:CoF) and corresponding specific capacitance was 687.9 F/g. The peaks in the forward scan were located at 0.26/ 0.64 V, whereas those in the reverse scan were present at 0.29/0.07 V, respectively. For PANI/AC/CuF, the optimized composition obtained was 4:1:3 (PANI/AC/CuF) and corresponding specific capacitance was 816.4 F/g. The observed oxidation peaks occurred at 0.21 V, 0.32 V and 0.73 V and the reduction peaks were present at 0.10 V, 0.25 V and 0.40 V. The benzoquinone/hydroquinone transition peak is not present in the ternary composites' CV curves which may be due to interactions of AC and bimetallic oxide particles. The rod-like PANI structures combined with porous AC and dispersed bimetallic oxide particles provide

conductive interconnected networks. The synergistic effects of the individual constituents led to the enhancement in electrochemical performance of the ternary composite materials. In the case of PANI/AC/CuCO and PANI/AC/CoF, no significant difference in the specific capacitance was observed which may be due to the comparable crystalline sizes of the bimetallic oxides CuCo and CoF. A high specific capacitance was observed in the case of PANI/AC/CuF which may be due to much lower crystalline size of CuF. This lower crystalline size helps in improved interactions, offers greater dislocation density and grain boundary and eventually more sites for electrochemical reactions as discussed earlier.

6.8 Conclusion:

In the current research, the composite material based on polyaniline, activated carbon, and copper ferrite (PANI/AC/CuF) has been optimized based on varying weight ratios of AC and CuF with the help of Response Surface Methodology (RSM). The composite material with the proportion of 4:1:3 weight ratio of polyaniline, activated carbon, and copper ferrite shows excellent specific capacitance of 816.8 F/g in three-electrode configuration. The optimized ternary composite material demonstrated the highest specific energy density of 53.0 Wh/kg and specific power of 6000.1 W/kg. It also exhibited excellent capacitance retention of 87.1 % after 2500 cycles. The charge transfer resistance of the optimized ternary composite material PANI/AC/CuF was 4.82 Ω. Therefore, it can be concluded that on the basis of specific capacitance values, the optimized ternary composite material with a weight ratio of 4:1:3 (PANI:AC: CuF) was found to be the best material among all the prepared ternary composites for supercapacitor applications. Further, a short comparison of electrochemical performance of optimized ternary composite materials has been discussed.